Title: Intermittent fasting promotes ILC3s secreting IL-22 contributing to the beigeing of white adipose tissue.

Running Title: ILC3s and beigeing

Authors: Hong Chen[1,4#], Lijun Sun[1#], Lu Feng[1], Xue Han[1], Yunhua Zhang[1], Wenbo Zhai[1], Zehe Zhang[1], Michael Mulholland[2], Weizhen Zhang[1,2*], Yue Yin[3*]

Affiliations:

1. Department of Physiology and Pathophysiology, School of Basic Medical Sciences, and Key Laboratory of Molecular Cardiovascular Science, Ministry of Education, Peking University, Beijing 100191, China
2. Department of Surgery, University of Michigan Medical Center, Ann Arbor, MI 48109-0346, USA
3. Department of Pharmacology, School of Basic Medical Sciences, and Key Laboratory of Molecular Cardiovascular Science, Ministry of Education, Peking University, Beijing,100191, China.
4. State Key Laboratory of Female Fertility Promote, Center for Reproductive Medicine, Department of Obstetrics and Gynecology, Peking University Third Hospital, Beijing, China.

# These authors contribute equally to the study

***Correspondence:**

Weizhen Zhang

Department of Physiology and Pathophysiology, School of Basic Medical Sciences, Peking University Health Science Center, Beijing 100191, China

E-mail: weizhenzhang@bjmu.edu.cn; Tel: 0086-10-82802183

or

Yue Yin

Department of Pharmacology, School of Basic Medical Sciences, and Key Laboratory of Molecular Cardiovascular Science, Ministry of Education, Peking University, Beijing,100191, China.

E-mail: yueyin@bjmu.edu.cn; Tel: 0086-10-82802514

Author contributions

Weizhen Zhang, Yue Yin and Hong Chen designed the study; Hong Chen and Lijun Sun performed most of the experiments and analyzed the data; Lu Feng, Xue Han, Yunhua Zhang, Wenbo Zhai and Zehe Zhang helped with the experiments; Hong Chen wrote the original draft; Weizhen Zhang reviewed and edited the manuscript; Yue Yin and Weizhen Zhang obtained funding and supervised the study. All authors have read and agreed to the published version of the manuscript.

Competing interests

The authors declare no competing interests.

Acknowledgments

This research was supported by grants from the National Natural Science Foundation of China (81930015, 81730020, 82070592 and 82270610) and National Institutes of Health Grant R01DK112755 and 1R01DK129360.

Data availability

Data that support the findings in this study are available from corresponding authors upon reasonable request.

Abstract

Mechanism underlying the metabolic benefit of intermittent fasting remains largely unknown. Here, we reported that intermittent fasting promoted IL-22 production by ILC3s and subsequent beigeing of subcutaneous white adipose tissue. Adoptive transfer of intestinal ILC3s increased beigeing of white adipose tissue in diet-induced-obese mice. Exogenous IL-22 significantly increased the beigeing of subcutaneous white adipose tissue. Deficiency of IL-22 receptor attenuated the beigeing induced by intermittent fasting. Single-cell sequencing of sorted intestinal immune cells revealed that intermittent fasting increased aryl hydrocarbon receptor signaling in ILC3s. Analysis of cell–cell ligand receptor interactions indicated that intermittent fasting may stimulate the interaction of ILC3s with dendritic cells (DCs) and macrophages. These results establish the role of intestinal ILC3s in beigeing of white adipose tissue, suggesting that ILC3/IL-22/IL-22R axis contributes to the metabolic benefit of intermittent fasting.

Key word:

ILC3s; IL-22; Beigeing of white adipose tissue; Intermittent fasting

Introduction

Obesity is defined as an epidemic metabolic disease characterized by excessive fat accumulation as the consequence of long-term energy surplus. Thus, therapeutic management of obesity has been focused on the restoration of energy balance, either by decreasing energy intake or increasing energy expenditure[1]. Among these strategies, intermittent fasting is becoming a popular dietary approach. All intermittent fasting schemes including alternate day fasting, 5:2 intermittent fasting and daily time-restricted feeding have shown the health benefits such as delaying aging[2-6], improving metabolism[7, 8], and enhancing cognition[9-11]. The mechanism underlying metabolic benefit of intermittent fasting remains largely unknown. Its metabolic benefit was initially attributed to limitation of energy intake. Recent studies have indicated an alternative mechanism involving beigeing of white adipose tissue, which accounts for the major plasticity of energy expenditure. Studies by Kim *et al.* have showed that intermittent fasting induces white adipose beigeing via stimulation of angiogenesis and macrophage M2 polarization[12]. On the other hand, studies by Li *et al.*[13] have indicated that alternate day fasting induces white adipose tissue beigeing by shaping the gut microbiota and elevating the fermentation products acetate and lactate. Although gut microbiota is closely related to immune response, it remains unclear whether intestinal immune cells contribute to the metabolic benefit of intermittent fasting.

Innate lymphoid cells (ILCs) are a group of natural immune cells lacking antigen-specific receptors expressed on T cells and B cells[14]. Based on developmental trajectories, ILCs are divided into five groups: natural killer cells, type 1 ILCs, type 2

ILCs, type 3 ILCs (ILC3s) and lymphoid tissue-inducing cells[15]. Adipose-Resident type 1 ILCs can promote adipose tissue fibrosis and obesity-associated insulin resistance[16, 17] while type 2 ILCs promote beiging of white adipose tissue and limit obesity[18-20]. However, the contribution of ILC3s on adipocytes and obesity are less clear. ILC3s can produce interleukin-17 (IL-17) and interleukin-22 (IL-22) in response to extracellular bacteria and fungi[21]. ILC3s derived IL-22 can enhance the intestinal mucosal barrier function, reduce endotoxemia and inflammation, ameliorate insulin sensitivity[22, 23] and improve the metabolic disorder of polycystic ovary syndrome[24]. However, ILC3s are also reported to be involved in the induction of obesity[25], contributing to the metabolic disease [25-28]. Therefore, the role of ILC3s in metabolic disease seems complex and the role of ILC3s in intermittent fasting and beigeing of adipose tissue is not known.

Here, we showed that alternate day fasting promoted the secretion of IL-22 by ILC3s. Further, adoptive transfer of intestinal ILC3s increased thermogenesis in DIO mice. Exogenous IL-22 induced the beigeing of white adipose tissue. Deficiency of IL-22 receptor attenuated the beigeing of white adipose tissue induced by intermittent fasting. Our study demonstrates that intestinal ILC3-IL-22-IL-22R axis is actively involved in the regulation of adipose tissue beigeing. Our findings thus reveal a novel pathway in the dialog between the gut and adipose tissue.

Results

1. Intermittent fasting enhances IL-22 production by intestinal ILC3s

111 To explore the effect of intermittent fasting on intestinal immune cells, we applied
112 alternate-day fasting to mice fed normal chow diet (NCD-IF group) or high-fat diet
113 (HFD-IF group) (Fig. 1A). Intermittent fasting significantly reduced the body weight
114 of mice fed HFD, while demonstrating no effect on food intake rate which was
115 normalized to body weight (Supplementary Fig. 1A-B). Moreover, intermittent fasting
116 decreased the respiratory quotient (RQ) on the fasting day while increased the energy
117 consumption on the feeding day in mice fed HFD (Supplementary Fig. 1C, D),
118 improved glucose and lipid metabolism in mice fed HFD (Supplementary Fig. 1E, 1F),
119 and promoted white adipose tissue beigeing in mice fed NCD or HFD (Supplementary
120 Fig. 2).

121 To explore whether gut immune system contributes to the effects of intermittent
122 fasting on white adipose tissue beigeing, we examined levels of various cytokines in
123 intestine. Notably, mRNA level of IL-22 in the NCD-IF group was significantly higher
124 relevant to the control group (Fig. 1B). Consistently, plasma concentration of IL-22
125 detected by ELISA was also increased (Fig. 1C). These results suggest that intermittent
126 fasting increases levels of IL-22 in the intestine and plasma. Since ILC3s are the main
127 source of IL-22 in the small intestine[29-31], we detected the proportion of ILC3s in the
128 lamina propria of small intestine using flow cytometry. In mice fed NCD, intermittent
129 fasting significantly increased proportion of IL-22 positive ILC3s in the small intestine
130 lamina propria (Fig. 1D), while demonstrating no effect on the percentile of total ILC3s
131 (Fig. 1E). Interestingly, intermittent fasting did not influence the secretion of IL-22 of
132 T cells marked as Lineage^{+} Rorγ^{+} cells (Fig. 1F). Besides, intermittent fasting didn't

133 alter the levels of ILC3s and IL-22 in mouse adipose tissue (Fig. 1G and Supplementary
134 Fig. 3). Similar to NCD mice, intermittent fasting significantly increased mRNA levels
135 of IL-22 in the intestine of HFD mice while didn't influence the secretion of IL-22 by
136 T cells (Figure 1H-I). Furthermore, mice fed high-fat diet showed an obvious reduction
137 in the plasma IL-22 (Fig. 1J)and percentage of total and IL-22 positive ILC3s (Fig. 1K).
138 Further, the decrement of plasma IL-22 (Fig. 1J) as well as IL-22 positive ILCs in
139 intestine (Fig. 1K) was attenuated by 30 days intermittent fasting.

140 In order to explain the chronological relationship between ILC3s secreting IL-22
141 and beigeing of white adipose tissue, the mice were exposed to one cycle of intermittent
142 fasting for 2 days. At this time, the body weight of mice didn't change and beige
143 adipocytes haven't been induced (supplementary Fig 4 A-B). However, significant
144 increase in proportion of IL-22 positive ILC3s was induced by intermittent fasting for
145 two days whereas total percentile of ILC3s remained unalterd (supplementary Fig 4 C).
146 These results indicate that the beiging of white adipose tissue are subsequent to its effect
147 on ILC3s secreting IL-22.

148 2. Intestinal ILC3s promote beigeing of white adipose tissue

149 Next, we examined whether adoptive transfer of intestinal ILC3s can increase
150 beigeing of white adipose tissue in diet-induced obesity (DIO) mice. Intestinal ILC3s
151 were isolated and purified from the small intestinal lamina propria of NCD mice
152 (Supplementary Fig. 5A). These cells were defined as lineage^{-}CD127^{+}KLRG1^{-}c-Kit^{+}
153 cells (Supplementary Fig. 5B). As shown in Fig. 2A, DIO mice transferred with ILC3s
154 demonstrated a significant increment in the proportion of small intestinal ILC3s.

155 Previous researches report that intestinal ILC3s specifically express gut homing
156 receptors CCR7, CCR9, and α4β7[32-34], which may explain transplantation of intestinal
157 ILC3s can migrate mainly to the intestine instead of adipose tissue. Plasma
158 concentration of IL-22 also increased significantly relevant to PBS control (Fig. 2B).
159 Relevant to PBS control, adoptive transfer of intestinal ILC3s decreased body weight
160 and weight of sWAT (Subcutaneous adipose tissue) slightly, while had no impact on
161 food intake and the liver weight (Supplementary Fig 5C-E). In addition, ILC3s from
162 CD45.1 mouse intestinal lamina propria lymphocytes were adoptively transferred into
163 recipient mice, and CD45.1 positive immune cells were significantly increased in
164 intestine but not in adipose tissue in mice transferred with ILC3s (Supplementary Fig.
165 5E), indicating the feasibility of ILC3s adoptive transfer. Notably, DIO mice transferred
166 with intestinal ILC3s showed improved glucose tolerance (Fig. 2C) and decreased
167 levels of random blood glucose (Fig. 2D). Cold exposure experiment showed that DIO
168 mice transferred with intestinal ILC3s maintained significantly higher rectal
169 temperatures during a 6-h cold challenge (Fig. 2E). Consistently, key thermogenic
170 genes in sWAT including *Ucp1* and *Cidea* were significantly increased (Fig. 2F). Size
171 of adipocytes in the sWAT and eWAT was markedly reduced (Fig. 2G-H). Furthermore,
172 differentiated SVF cells co-cultured with intestinal ILC3s in vitro (Fig. 2I)
173 demonstrated a significant increment in the expression of *Ucp1* and *Pparg* (Fig. 2J), as
174 well as a concurrent decrement in the size of lipid droplets (Fig. 2K). On the other hand,
175 co-culture with $CD127^-$ cells demonstrated no effect (Fig. 2J-K). The in vitro
176 experiment indicates the direct effect of ILC3s on adipocytes.

3. Exogenous IL-22 increases beigeing of white adipose tissue

The role of type 3 immunity in DIO and metabolic syndrome is complex. ILC3-derived IL-22 are beneficial in metabolic syndrome[22, 35] but can also contribute to metabolic disease[25-27]. In order to examine the role of promoting beigeing of white adipose tissue of IL-22 in the context of NCD and HFD mice, we intraperitoneally administrated IL-22 at the dose of 4 μg/kg body weight/every other day for 6 weeks into mice fed NCD or HFD. Saline was used as control. Administration of IL-22 increased its plasma concentration in mice fed either NCD or HFD (Supplementary Fig. 6A). Exogenous IL-22 significantly increased oxygen consumption, carbon dioxide production and energy expenditure in mice fed either NCD or HFD (Fig. 3A-F). Respiratory quotient (RQ) was significantly reduced in mice fed NCD at dark and mice fed HFD at light(Fig. 3G-H). No significant difference was observed for animal activity (Supplementary Fig. 6B). In addition, exogenous IL-22 significantly improved glucose tolerance in mice fed HFD (Fig. 4A). Interestingly, body weight and food intake were not altered (Supplementary Fig. 6C-6D), indicating that the metabolic benefit of IL-22 is not dependent on food intake. Consistent with previous research, IL-22 administration improves insulin sensitivity without change in body weight[36]. In addition, IL-22 can increase Akt phosphorylation in muscle, liver and adipose tissues, leading to improvement in insulin sensitivity[22].

We next explored the effect of exogenous IL-22 on thermogenesis induced by 4°C cold exposure. Exogenous IL-22 rendered mice fed HFD resistant to core temperature drop induced by cold exposure (Fig. 4B). Relevant to the pale yellow color in the

199 control animals, subcutaneous fat of obese mice treated with exogenous IL-22 appeared
200 dark yellowish (Fig. 4C). The mRNA levels of thermogenic genes such as *Ucp1* were
201 significantly increased by IL-22 (Fig. 4D). Adipocyte size of subcutaneous adipose
202 tissue and epididymal adipose tissue was significantly reduced in the animals treated
203 with IL-22 (Fig. 4E-4F). These observations suggest that intraperitoneal injection of
204 IL-22 promotes the beigeing of white adipose tissue in mice.

205 To determine whether IL-22 can directly act on adipocytes to promote their beigeing,
206 adipose tissue SVF was isolated and induced for beige differentiation. Il22ra1 mainly
207 expressed on mature adipocytes (Supplementary Fig. 6E). IL-22 at the dose of 100
208 ng/mL was continuously administered during beige differentiation. IL-22 significantly
209 increased SVF beige differentiation evidenced by cell morphology, increment in mRNA
210 levels of genes relevant to thermogenesis, including *Ucp1* and *Cidea*, and protein level
211 of UCP1(Fig. 4G-I, Supplementary Fig. 6E). IL-22 did not alter the levels of genes
212 related to adipogenesis (Supplementary Fig. 6F). As expected, IL-22 increased the
213 phosphorylation of STAT3 and MAPK (Fig.4I, Supplementary Fig. 6G), which can
214 increase the expression of thermogenic genes[37, 38]. These results suggest that IL-22 can
215 directly stimulate beigeing of white adipose tissue.

216 4. IL-22R knock-out blocks beigeing induced by intermittent 217 fasting

218 To explore whether IL-22R mediates the effect of intermittent fasting on the beigeing
219 of white adipose tissue, IL-22R knockout (IL-22RKO) mice and wild-type (WT)
220 littermates were subjected to alternate-day fasting diet for 30 days. Rectal temperature

221 of WT-IF and IL-22RKO-IF mice was monitored during two consecutive days of
222 intermittent fasting. On the fasting day, the rectal temperature of IL-22RKO-IF mice
223 was significantly lower than that of WT-IF mice at 16:00 time point (Fig. 5A). On the
224 feeding day, the rectal temperature of IL-22RKO-IF mice was lower at three time points:
225 8:00, 12:00 and 20:00 (Fig. 5B). These results indicate that IL-22RKO attenuates the
226 thermogenesis induced by intermittent fasting. Knock-out of IL-22R demonstrated no
227 effect on the glucose tolerance and insulin sensitivity in mice fed NCD (Fig. 5C-D).
228 However, the weight of subcutaneous adipose tissue in IL-22RKO-IF mice increased
229 significantly (Fig. 5E). mRNA levels of the thermogenic gene *Ucp1* decreased
230 substantially, whereas *Fabp4* increased (Fig. 5F). Furthermore, knockout of IL-22R
231 significantly attenuated the increment of multilocular lipid droplets and the decrement
232 of adipocyte size in the subcutaneous fat induced by intermittent fasting (Fig. 5G-H),
233 indicating a reduction in beigeing.

234 To further explore whether IL-22R mediates the effect of ILC3s on beigeing of
235 adipocytes, intestinal ILC3s isolated from intermittent fasting mice were co-cultured
236 with beige adipocytes from subcutaneous SVF of WT or IL-22RKO mice (Fig. 5I-J).
237 Co-culture with ILC3s significantly increased the mRNA levels of thermogenic genes
238 in beige adipocytes derived from WT mice, while demonstrating no effect on beige
239 adipocytes derived from IL-22RKO mice (Fig. 5K). These observations indicate that
240 IL-22R mediates the effect of intestinal ILC3s on beigeing of white adipocytes.

241 5. Profiling of intestinal immune cells in mice fed NCD, HFD or 242 HFD-IF

To explore the mechanism by which intermittent fasting promotes the secretion of IL-22 by ILC3s, live $CD45^+$ Lineage (CD3, CD5, B220, CD19, Gr1)$^-$ cells isolated from the siLP of mice fed NCD, HFD or HFD-IF were subjected for single-cell sequencing (Supplementary Fig. 7A). Following quality controls, we analyzed 7455, 4803, 5954 single cells for the NCD, HFD and HFD-IF groups using Seurat-V3.1, respectively. Based on singleR, we identified twenty-five distinct clusters of immune cells (Fig. 6A and Supplementary Fig. 7B), including ILC1s (Cluster 7 and cluster 16), ILC2s (Cluster 2, cluster 12, cluster 13, and cluster 14), ILC3s (cluster 3 and cluster 5), dendritic cells (Cluster 1, cluster 4, cluster 9, cluster 10, cluster 11, cluster 17, cluster 18, and cluster 21), eosinophils (Cluster 0 and cluster 6), B cells (Cluster 8 and cluster 24), macrophages (Cluster 15, cluster 20, and cluster 23), NKT cells (Cluster 22) and mast cells (Cluster 19). As expected, ILC3s expressed high RNA levels of Il7r (CD127), Rorc, and IL-22 (Fig. 6B, C and Supplementary Fig. 7C, D). ILC3s contain two distinct cell types with highly similar expression profiles: NCR^+ and NCR^-. These ILC3s were distinguished in our analysis as Cluster 5 and Cluster 3 respectively. NCR^- ILC3s (cluster 3) were CCR6 positive and contained lymphoid tissue inducer (LTi) cells (Fig. 6B). Interestingly, NCR^- ILC3s were characterized by high levels of vasoactive intestinal peptide receptor 2 (Vipr2) (Fig. 6C), which is critical for the migration and function of ILC3s[29, 39, 40]. The heatmap of cellular composition showed the differences in cell number and percentage among NCD, HFD and HFD IF mice (Supplementary Fig. 8A). The change in ILC3 number was consistent with the flow cytometry results. The percentage of IL-22^+ cells in NCR^+ ILC3s was significantly increased by IF in mice

265 fed HFD (Supplementary Fig. 8B). Moreover, GSEA revealed that HFD-induced
266 decrement of cytokine–cytokine receptor interaction, in which IL-22 is included, was
267 reversed by IF (Supplementary Fig. 8C). Besides, Neuroactive ligand-receptor
268 interaction, in which vipr2 is included, was up-regulated in HFD-IF (Supplementary
269 Fig. 8D). The mRNA levels of *Vipr2* had a tendency to increase in in sorted ILC3s from
270 the small intestine of HFD IF mice compared with that of HFD mice (Supplementary
271 Fig. 8E). Further, gene difference analysis revealed that HFD-induced increase of
272 Zmat4 was significantly attenuated by IF (Fig. 6D, Supplementary Fig. 8F-G).

273 Further, the expression level of Hsp90ab1 in both NCR^- ILC3s and NCR^+ was
274 significantly increased by IF in mice fed HFD (Fig. 6D, Supplementary 10H).
275 Transcription factor analysis using the JASPAR database and TFBS Tools revealed that
276 the expression of *Hsp90ab1* may be regulated by aryl hydrocarbon receptor (AHR) (Fig.
277 6D). AHR is located in the Hsp90:XAP2:p23:Src chaperone protein complex in the
278 cytoplasm without stimulation. Upon binding with the ligand, AhR translocates to the
279 nucleus and heterodimerizes with AhR nuclear translocator (ARNT) to control the
280 transcription of target genes, including AhR repressor (*Ahrr*), *Cyp1a1*, *Cyp1b1* and
281 *Il22*[41]. Consistently, Gene Ontology analysis of the top 20 increased difference genes
282 revealed that aryl hydrocarbon receptor signaling was one of the key pathways affected
283 by intermittent fasting in HFD mice (Fig. 6E-F). Furthermore, the AHR target genes,
284 including *Il22*, *Ahrr*, *Cyp1a1*, *Cyp1b1*, increased significantly in ILC3s sorted from
285 HFD-IF mice compared with HFD mice. These results indicates that intermittent fasting
286 increases the production of IL-22 likely via activation of AhR.

287 **6. IF ameliorates the impaired interaction between intestinal**
288 **myeloid cells and ILC3s**

289 Because dendritic cells (DCs) can influence the production of IL-22 by ILC3s, we
290 next analyzed the change in DCs induced by intermittent fasting. IF significantly
291 attenuated the increment of inflammatory factors, such as Ccl4, Ccl17 and Ccl22, of
292 DCs in mice fed HFD (Fig. 7A). Kyoto Encyclopedia of Genes and Genomes (KEGG)
293 analysis of the top 20 differentially expressed genes in cluster 17 revealed that the
294 increase of inflammation-related pathways induced by HFD was obviously attenuated
295 by IF (Fig. 7B-C). These observations indicate that intermittent fasting may ameliorate
296 the inflammatory state of the intestine by decreasing the NOD-like receptor signaling
297 pathway in DCs (Fig. 7B-C).

298 We next analyzed the intestinal cellular communication networks using CellPhone
299 DB analysis based on homologous gene transformation on all immune cells acquired.
300 CellPhone DB ligand–receptor analysis revealed hundreds of immune-to-immune
301 interactions (Supplementary Fig. 9A). Connectome web analysis of siLP immune cells
302 revealed strong interactions among $CD8^+$ dendritic cells (DC) (Cluster 4), $CD127^+$
303 ILC1s (Cluster 16), $DC8^-$ DC-1 (Cluster 9), Macrophages-1 (Cluster 15), $CD8^-$ DC-2
304 (Cluster 1), Macrophages-2 (Cluster 23), $CD8^-$ DC-3 (Cluster 10), $CD8^-$ DC-4 (Cluster
305 11), and $CD8^-$ DC-5 (Cluster 17). Notably, NCR^+ ILC3s strongly interacted with $CD8^+$
306 dendritic cells (DC) (Cluster 4), $CD127^+$ ILC1 s (Cluster 16), $DC8^-$ DC (Cluster 9),
307 macrophages (Cluster 15), $CD8^-$ DC (Cluster 1), macrophages (Cluster 23), $CD8^-$ DC
308 (Cluster 10), $CD8^-$ DC (Cluster 11), and $CD8^-$ DC (Cluster 17). ILC subsets, DCs and

309 macrophages were in the central communication hubs of the healthy small intestine
310 (Supplementary Fig. 9B-C). Analysis of highly expressed interactions uncovered
311 various uncharacterized and validated signaling pathways implicated in intestine
312 homeostasis in mice (Supplementary Fig. 9D). Analysis of the NCD mouse interactome
313 suggests that macrophages (cluster 15) may interact with NCR^+ ILC3s through
314 CD74_COPA, CD74_MIF, CD44_HBEGF, CD44_FGFR2, CCL4_SLC7A1, and
315 IL1B_ADRB2. Similarly, DCs (cluster 9) may interact with NCR^+ILC3s through
316 CD74_COPA, CD74_MIF, IL1B_ADRB2, CD44_HBEGF, and CD44_FGFR2. All
317 these observations indicates that macrophages and DCs play critical roles in the
318 recruitment and maintenance of ILC3s.

319 HFD significantly reduced the interaction between ILC subsets, DCs and
320 macrophages in the small intestine (Fig. 7D and Supplementary Fig. 9B). This reduction
321 was reversed by IF (Fig. 7E and Supplementary Fig. 11B). Analysis of the interactomes
322 in mice fed HFD suggested that IF significantly altered the interacting proteins (Fig.
323 7F-G). To further test this observation, we sorted macrophages and ILC3s from HFD
324 and HFD-IF mice (Supplementary Fig. 10A). As shown in supplementary Fig. 10B-C,
325 *Ccl4* and *Cd74* increased significantly in macrophages, while the receptors expressed
326 on ILC3s remained largely unchanged. Together, these data suggest that IF may
327 promote the production of IL-22 from ILC3s by altering the interactome in intestinal
328 myeloid cells and ILC3s.

329 Discussion

330 Our present study demonstrates that intestinal ILC3s are critical for the beigeing of

331 white adipose tissue induced by intermittent fasting. This conclusion is supported by
332 following observations. Firstly, intermittent fasting stimulates the secretion of IL-22 by
333 intestinal ILC3s in either lean mice fed normal chow diet, obese mice fed high-fat diet
334 mice, or mice with metabolic dysfunction induced by HFCD diet. Secondly, a
335 comprehensive set of in vivo and in vitro experiments shows that intermittent fasting
336 promotes adipose tissue beigeing through the intestinal ILC3-IL-22-IL-22R axis.

337 The role of ILC3s in metabolism remains largely unknown. Our studies provide
338 evidence supporting the metabolic benefit of intestinal ILC3s in intermittent fasting.
339 Adoptive transfer of intestinal ILC3s isolated from lean mice was sufficient to improve
340 the metabolic dysfunctions in DIO mice, including increase of white adipose tissue
341 beigeing and glucose tolerance. Interestingly, adoptive transfer of ILC3s significantly
342 increased their number only in intestine. Further, alternate day fasting did not alter the
343 ILC3s in adipose tissue. These observations indicate that ILC3s in intestine rather than
344 in adipose tissue account for the metabolic benefit. In addition to directly promoting
345 the beigeing of white adipose tissue through IL-22, intestinal ILC3s may enhance the
346 intestinal mucosal barrier[42], reducing serum LPS and peptidoglycan, thus reducing the
347 inhibitory effect of LPS and peptidoglycan on the beigeing of white adipose tissue[43].
348 O'Sullivan et al.[16] have reported that ILC3s are negligible in white adipose tissue of
349 either lean or obese mice. Similarly, Sasaki *et al.*[25] have demonstrated that
350 transplanting bone marrow cells from Rag2$^{-/-}$ mice (lack of T cells, B cells) into Il2rg$^{-/-}$
351 Rag2$^{-/-}$ mice (lack of T cells, B cells, ILC cells) could not increase the number of ILC3s
352 in the adipose tissue of recipient mice. However, it is worth of noting that ILC3s have

353 been detected in adipose tissue by other report. Using the marker Lineage$^-$KLRG1$^-$Il-
354 7rα$^+$Thy-1$^+$, ILC3s cells have been reported to account for approximately 20% of
355 lineage$^-$KLRG1$^-$Il-7rα$^+$ cells in adipose tissue. In our study, we also detected ILC3s
356 defined as CD127$^+$Lin$^-$RORγt$^+$ in adipose tissue. These ILC3s accounted for
357 approximately 10% of CD127$^+$Lin$^-$ cells. ILC3s have also been shown to be present in
358 human adipose tissue[44]. Importantly, the proportion and density of ILC3s in white
359 adipose tissue of people with obesity increase relevant to healthy people, and positively
360 correlate with BMI in obese patients. Thus, the existence and function of ILC3s in
361 mouse and human adipose tissue deserve further investigation.

362 Communication between intestine and metabolic organs is currently under active
363 investigation. Our studies identify ILC3s-IL-22-IL-22R as a novel pathway medicating
364 the crosstalk between intestine and adipose tissue. Evidence supporting this conclusion
365 are five folds. (1) Intermittent fasting reverses the reduction of intestinal ILC3s and IL-
366 22 in DIO mice. (2) Adoptive transfer of intestinal ILC3s enhances beigeing of white
367 adipose tissue. (3) Co-culture of intestinal ILC3s with SVF cells increases their
368 differentiation into beige cells. (4) Exogenous IL-22 mimics the effect of intermittent
369 fasting on beigeing of white adipose tissue. (5) Deficiency of IL-22R blocks the IF-
370 induced beigeing of white adipose tissue. In lines with our observation, a series of
371 recent studies have suggested that cytokines can act directly on adipocytes to regulate
372 thermogenesis. For example, γδ T cells regulate heat production by secreting IL-17[45].
373 Deficiency of IL-10 increases energy consumption and renders mice resistant to diet-
374 induced obesity[34]. IL-27-IL-27Rα signaling promotes thermogenesis, prevents diet-

375 induced obesity, and improves insulin resistance[46]. IL-33 induces the beigeing of white
376 adipose tissue by activating ILC2s[18]. Our studies extend the effect of cytokines on
377 thermogenesis to IL-22. IL-22 promotes heat production, renders mice resistant to
378 reduction of body temperature induced by cold exposure, and reduces obesity induced
379 by high-fat diet. Together with previous report showing that IL-22 increases the
380 lipolysis of adipocytes, our studies suggest that IL-22 can directly act on adipocytes to
381 alter the adipose tissue homeostasis. IL-22 activates IL-22 receptor, which then
382 regulates the expression of downstream inflammatory factors, tissue repair molecules,
383 chemokines, antimicrobial peptides and other molecules via Jak-1 and Tyk-2 dependent
384 phosphorylation of STAT3. Our studies suggest that IL-22 may promote the expression
385 of downstream thermogenic genes in adipose tissue through IL-22R. Deficiency of IL-
386 22R blocks the up-regulation of thermogenic genes induced by intermittent fasting.
387 SVF cells lacking IL-22R demonstrate no response to the up-regulation of thermogenic
388 genes induced by intestinal ILC3. Thus, our results provide novel evidence supporting
389 the concept that intestinal ILC3s modulate beigeing of adipose tissue via IL-22-IL-22R
390 pathway.

391 The physiological mechanism underlying the secretion of IL-22 by ILC3s remains
392 largely unknown. Our studies reveal the distinct secretion pattern of IL-22 induced by
393 intermittent fasting. Consistently, previous studies have shown that secretion of IL-22
394 by ILC3s changes between active and quiescent periods throughout the day which is
395 regulated by the cycle patterns of food intake[47]. These suggest that secretion of IL-22
396 by ILC3s is altered by feeding rhythm. It is currently unclear how feeding influences

397 the physiological function of ILC3s. Previous studies indicate a mechanism involving
398 neuropeptide vasoactive intestinal peptide (VIP), which is able to stimulate the
399 secretion of IL-22 by ILC3s[29]. Consistently, our single cell RNAseq data also
400 showedthat VIP receptor 2 (VIPR2) is highly expressed in intestinal ILC3s and
401 intermittent fasting activates VIPR2 signaling pathway. Since release of VIP is
402 stimulated by food intake, these observations indicate that VIP-VIPR signaling may
403 coordinate with food intake to drive the production of IL-22. However, conflicting
404 result exists. Studies by Talbot *et al* have shown that VIP inhibits ILC3 secretion of IL-
405 22[39]. Reasons accounting for this difference remains unknown but may be context
406 dependent. Alternatively, we found that intermittent fasting may promote ILC3s
407 secreting IL-22 though activating AhR signaling. In addition, feeding may decrease the
408 levels of antimicrobial peptides secreted by epithelial cells, while increasing the
409 expression of lipid-binding proteins[39]. Moreover, segmented filamentous bacteria may
410 account for the effect of feeding on the secretion of IL-22 by intestinal ILC3s by
411 periodically attaching to the epithelial surface[47]. These alterations may substantially
412 influence the immune networks in intestine, leading to subsequent change in the
413 secretion of IL-22 by ILC3s. In support of this concept, our single cell RNAseq analysis
414 shows a significant change in the intestinal immune cell network involving dendritic
415 cells, macrophages and ILC3s. Further examination should focus on dissecting the
416 novel molecular mechanism by which intestinal dendritic cells and macrophages
417 interact with ILC3s and its consequence on the IL-22 production.

418 In conclusion, our studies suggest that intermittent fasting can promote the secretion

419 of IL-22 by intestinal ILC3s. IL-22 promotes beigeing of white adipose tissue through
420 IL-22R. Intestinal ILC3s thus may serve as a potential target for the intervention of
421 metabolic disorders.

422 # Materials and Methods

423 ## 1. Animals

424 Four-week-old male C57BL/6 and CD45.1 mice were obtained from Charles River
425 Laboratories (Peking, China). IL-22 receptor knockout mice (IL-22R KO mice, KO-
426 00115) were purchased from BRL Medicine Inc. Mice were handled in accordance with
427 the Guide for the Care and Use of Laboratory Animals prepared by the National
428 Academy of Sciences and published by the National Institutes of Health (NIH
429 publication 86-23, revised 1985). Mice were housed in standard rodent cages and
430 maintained in a regulated environment (21-24°C, humidity at 40-70%, 12:12 h light :
431 dark cycle with lights on at 8:00 AM). A normal chow diet (D12450H; Research Diets)
432 and water were available ad libitum. Obese mice (DIO) were induced with a high-fat
433 diet (60% fat, D12492; Research Diets) for 12 weeks. Eight-week-old C57BL/6 mice
434 received intraperitoneal injection of saline control or IL-22 (R&D, 582-ML) at a dose
435 of 4 μg/kg/day every other day for 6 weeks. All experimental procedures were approved
436 by the Animal Care and Use Committee of Peking University.

437 ## 2. Cell preparation

438 For isolation of small intestine lamina propria cells, small intestines from
439 euthanized mice were emptied of the contents, excised of Peyer's patches, opened
440 longitudinally and cut into 1 cm pieces. The intraepithelial lymphocytes (IELs) were

441 dissociated from the intestine fragments by first shaking the fragments for 20 min at
442 37°C in PBS containing 0.3% BSA, 5 mM EDTA and 1 mM dithiothreitol. Vortex the
443 fragments three times with PBS containing 2 mM EDTA. To isolate lamina propria cells,
444 the remaining fragments were minced and digested at 37°C for 50 min in RPMI 1640
445 medium containing 0.04 mg/mL collagenase IV (Sigma), 0.1 mg/mL
446 deoxyribonuclease (DNase) I (Roche), and 0.5 mg/mL dispase. The digestion
447 suspension was then filtered through a 40 μm cell strainer and centrifuged at 540 g for
448 6 min. Cell pellets were resuspended in PBS containing 2% FBS for further analysis.

449 **3. Flow cytometry**

450 Single-cell suspensions were preincubated with anti-CD16/32 (clone 2.4G2) for 10
451 min to block the surface Fc receptors. Then, cell-surface molecules were stained with
452 different antibody combinations for 30 min in cell staining buffer. Dead cells were
453 excluded with Fixable Viability Dye eFluor^{TM} 606 (Invitrogen). For intracellular
454 transcription factor staining, the cells were fixed and permeabilized with a Foxp3
455 staining buffer set (eBioscience) according to the manufacturer's protocol.
456 Transcription factor staining usually lasted for more than 4 hours at 4°C. The gate
457 strategy for ILC3s was live lingeage (CD3, CD5, CD19, B220 and Gr-1)$^{-}$
458 CD127^{+}RORγt^{+}. For intracellular cytokine staining, the digested cells were first
459 incubated in RPMI 1640 with 10% FBS and 10 ng/ml recombinant murine IL-7
460 (PeproTech), and stimulated with 50 ng/ml phorbol 12-myristate 13-acetate, 750 ng/ml
461 ionomycin for 3 h and added with 2 μM monensin for the last 2.5 h.

462 Flow cytometry analyses were performed on an LSR Fortessa (BD Biosciences).

463 The flow cytometry data were analyzed with FlowJo software (Tree Star). The antibody
464 used in this study are listed in Supplementary Table 1.

465 4. ILC3s sorting, transfer and co-culture experiment

466 For ILC3s transfer experiment, co-culture experiment and single-cell RNA-Seq,
467 ILCs were collected by FACS. Small intestine lamina propria cells were prepared and
468 stained with surface molecules for 30 min at 4℃ followed by sorting on a FACS Aria
469 III cell sorter (BD Biosciences). A gating strategy of live Lineage^{-}CD127^{+}KLRG1^{-}c-
470 Kit^{+} was used to sort the ILC3s.

471 Purification checks were performed after each sort. The cells were suspended in
472 phosphate buffered saline（PBS）and then intravenously injected into HFD mice (200
473 μL PBS/mouse). ILC3s were sorted from 20 WT NCD mice, and sorting for the
474 adoptive transfer was performed six times within 4 weeks from the first injection. The
475 total number of ILC3 injected into HFD mice was 2.4×10^5 cells/mouse/experiment.
476 Mice were placed on an HFD for 16 weeks before ILC3s were transferred. In addition,
477 to confirm that these cells indeed originate from NCD mice, we transferred ILC3s from
478 CD45.1 mice to WT mice and detected the CD45.1 positive cells in recipient mice.

479 5. Single-cell RNA-Seq

480 Single cells were captured via the GemCode Single Cell Platform using the
481 GemCode Gel Bead, Chip and Library Kits (10X Genomics) according to the
482 manufacturer's protocol. Briefly, flow-sorted cells were suspended in PBS containing
483 0.4% BSA and loaded at 6,000 cells per channel. The cells were then partitioned into a
484 GemCode instrument, where individual cells were lysed and mixed with beads carrying

485 unique barcodes in individual oil droplets. The products were subjected to reverse
486 transcription, emulsion breaking, cDNA amplification, shearing, 5′ adaptor and sample
487 index attachment. Libraries were sequenced on a HiSeq 2500 (Illumina).

488 6. Isolation of stromal vascular fraction cells (SVF) and induction
489 of beigeing

490 Isolation of SVF and induction of beigeing were performed as reported[48]. Briefly,
491 subcutaneous white adipose tissue (sWAT) from male C57BL/6 mice was digested with
492 1 mg/mL type 2 collagenase (Sigma–Aldrich) at 37°C for 40 minutes with shaking.
493 Digestion was terminated by complete DMEM/F12 medium containing 10% fetal
494 bovine serum (FBS), 100 units/mL penicillin and 100 units/mL streptomycin
495 (Invitrogen, CA, USA). The cell suspension was centrifuged at 700×g for 10 minutes
496 to separate floating adipocytes from the SVF pellets. The pellets containing the SVF
497 cells were resuspended in complete medium and filtered using a 70 μm diameter filter.
498 The cell suspension was then centrifuged at 700×g for 10 minutes. Cell pellets were
499 resuspended and mixed well and then plated on dishes in complete medium. Cells were
500 grown to 95% confluence in complete medium and then differentiated into beige or
501 white adipocytes as previously described[49]. Briefly, for induction to beige adipocytes,
502 cells were cultured for 2 days with induction medium supplemented with 5 μg/mL
503 insulin, 1 nmol/L T3, 1 μmol/L rosiglitazone, 125 μmol/L indomethacin, 0.5 mmol/L
504 isobutylmethylxanthine (IBMX) and 5 μmol/L dexamethasone. Cells were then
505 cultured in maintenance medium supplemented with 5 μg/ml insulin, 1 nmol/L T3 and
506 1 μmol/L rosiglitazone for 4 days. Fresh media were replaced every 2 days.

507 ## 7. Co-culture experiments

508 To determine the direct effect of ILC3s on beige adipocytes differentiation, SVF
509 were co-cultured with ILC3s using a transwell system (0.4 μm pore size, BD
510 Biosciences). In brief, SVF isolated from adipose tissue were grown in the bottom
511 chamber of the transwell insert in a 12-well plate and induced into beige adipocytes,
512 while sorted ILC3s were seeded in the upper chamber. SVFs cultured alone and SVF
513 cells co-cultured with $CD127^-$ cells were used as controls. After co-culture for 72 h,
514 beige adipocytes in the lower chamber were collected for further detection.

515 ## 8. RNA isolation and qPCR analysis

516 RNA was extracted from cells or adipose tissue using RNATrip (Applied Gene,
517 Beijing, China) and reverse-transcribed into cDNAs with Hifair™ III 1st Strand cDNA
518 Synthesis SuperMix (Yeasen). SYBR Green-based quantitative real-time PCR was
519 performed using the Agilent Aria Mx real-time PCR system. The primer sequences used
520 in this study are listed in Supplementary Table 2.

521 ## 9. Western blot analysis

522 Differentiated SVF cells and sWAT were homogenized using RIPA lysis buffer.
523 Proteins were separated by 10% sodium dodecyl sulfate–polyacrylamide gel
524 electrophoresis and then transferred onto a nitrocellulose (NC) membrane. Membranes
525 were incubated in 5% fat-free milk for 1 hour at room temperature and then incubated
526 with primary antibodies overnight at 4°C. The reaction was detected with IRDye-
527 conjugated secondary antibody and visualized using the Odyssey infrared imaging
528 system (LI-COR Biosciences).

10. Histological studies

Paraffin-embedded sWAT sections were stained with hematoxylin-eosin (H&E). Images were scanned using a NanoZoomer-SQ (Hamamatsu).

11. Oil red O staining

Cells were washed with PBS for three times, and then fixed with 4% paraformaldehyde for 30 minutes. Next, the cells were stained with oil red O for 60 minutes, and washed with PBS for 5 minutes. Cells were then stained with hematoxylin for 5 seconds and washed with PBS. The dyed cells were photographed under the microscope (Leica, Germany).

12. Enzyme-linked immunosorbent assay

Levels of IL-22 were measured by double-antibody sandwich enzyme-linked immunosorbent assays (ELISAs) (M2200; R&D Systems). Briefly, 100 μL of Assay Diluent were added to each well. 50 uL of blood samples and standards were added and incubated at room temperature for 2 hours. After washing, conjugates were added and incubated for 2 hours. After washing, the substrate solution was added and incubated for 30 minutes and washed. And stop solution were added finally. Optical density (OD) values were measured using a microplate reader (Bio-Rad, Hercules, CA, USA).

13. OGTT and ITT

Oral Glucose tolerance tests (OGTT) and insulin tolerance tests (ITT) were performed after 16 or 6 hours of fasting, respectively. Mice were given with 3 g/kg glucose by gavage or injected intraperitoneally with 0.75 U/kg insulin. Blood samples were collected from the tail vain at 0, 15, 30, 60, 90 and 120 min after glucose or insulin

treatment. Blood glucose levels were measured using a glucometer (Roche, Basel, CH).

14. Cold exposure

Mice were placed in a 4°C cold room for 6 hours. The rectal temperature was measured every hour during the cold challenge with a rectal probe (Braintree Scientific, Braintree, MA).

15. Statistical analysis

Data were analyzed by GraphPad Prism software v.8.0 and presented as the mean ±s.e.m. The Shapiro–Wilk normality test was used to determine the normal distribution of samples. Unpaired Student's *t* test (normal distribution) or Mann–Whitney U-tests (non-normal distribution) was used to analyze data between two groups and one-way ANOVA followed by Bonferroni's multiple-comparisons test (normal distribution) or Kruskal–Wallis test (non-normal distribution) was used for three or more groups. The sample sizes were determined by power analysis using StatMate v.2.0. No data were excluded during the data analysis.

References Uncategorized References

[1] Liu B, Du Y, Wu Y, Snetselaar L G, Wallace R B, Bao W. Trends in obesity and adiposity measures by race or ethnicity among adults in the united states 2011-18: Population based study. Bmj. 2021, 372: n365

[2] Colman R J, Anderson R M, Johnson S C, Kastman E K, Kosmatka K J, Beasley T M, Allison D B, Cruzen C, Simmons H A, Kemnitz J W, Weindruch R. Caloric restriction delays disease onset and mortality in rhesus monkeys. Science (New York, N.Y.). 2009, 325(5937): 201-204

[3] Mattison J A, Roth G S, Beasley T M, Tilmont E M, Handy A M, Herbert R L, Longo D L, Allison D B, Young J E, Bryant M, Barnard D, Ward W F, Qi W, Ingram D K, de Cabo R. Impact of caloric restriction on health and survival in rhesus monkeys from the nia study. Nature. 2012, 489(7415): 318-321

[4] Mattison J A, Colman R J, Beasley T M, Allison D B, Kemnitz J W, Roth G S, Ingram D K, Weindruch R, de Cabo R, Anderson R M. Caloric restriction improves health and survival of rhesus monkeys. Nature Communications. 2017, 8: 14063

[5] Ulgherait M, Midoun A M, Park S J, Gatto J A, Tener S J, Siewert J, Klickstein N, Canman J C, Ja W W, Shirasu-Hiza M. Circadian autophagy drives iTRF-mediated longevity. Nature. 2021, 598(7880): 353-358

[6] Stekovic S, Hofer S J, Tripolt N, Aon M A, Royer P, Pein L, Stadler J T, Pendl T, Prietl B, Url J, Schroeder S, Tadic J, Eisenberg T, Magnes C, Stumpe M, Zuegner E, Bordag N, Riedl R, Schmidt A, Kolesnik E, Verheyen N, Springer A, Madl T, Sinner F, de Cabo R, Kroemer G, Obermayer-Pietsch B, Dengjel J, Sourij H, Pieber T R, Madeo F. Alternate day fasting improves physiological and molecular markers of aging in healthy, non-obese humans. Cell Metabolism. 2019, 30(3): 878-881

[7] de Cabo R, Mattson M P. Effects of intermittent fasting on health, aging, and disease. New England Journal of Medicine. 2019, 381(26): 2541-2551

[8] Hepler C, Weidemann B J, Waldeck N J, Marcheva B, Cedernaes J, Thorne A K, Kobayashi Y, Nozawa R, Newman M V, Gao P, Shao M, Ramsey K M, Gupta R K, Bass J. Time-restricted feeding mitigates obesity through adipocyte thermogenesis. Science. 2022, 378(6617): 276-284

[9] Mattson M P, Moehl K, Ghena N, Schmaedick M, Cheng A. Intermittent metabolic switching, neuroplasticity and brain health. Nature Reviews. Neuroscience. 2018, 19(2): 63-80

[10] Liu Y, Cheng A, Li Y-J, Yang Y, Kishimoto Y, Zhang S, Wang Y, Wan R, Raefsky S M, Lu D, Saito T, Saido T, Zhu J, Wu L-J, Mattson M P. Sirt3 mediates hippocampal synaptic adaptations to intermittent fasting and ameliorates deficits in app mutant mice. Nature Communications. 2019, 10(1): 1886

[11] Mattson M P, Arumugam T V. Hallmarks of brain aging: Adaptive and pathological modification by metabolic states. Cell Metabolism. 2018, 27(6): 1176-1199

[12] Kim K-H, Kim Y H, Son J E, Lee J H, Kim S, Choe M S, Moon J H, Zhong J, Fu K, Lenglin F, Yoo J-A, Bilan P J, Klip A, Nagy A, Kim J-R, Park J G, Hussein S M, Doh K-O, Hui C-C, Sung H-K. Intermittent fasting promotes adipose thermogenesis and metabolic homeostasis via VEGF-mediated alternative activation of macrophage. Cell Research. 2017, 27(11): 1309-1326

[13] Li G, Xie C, Lu S, Nichols R G, Tian Y, Li L, Patel D, Ma Y, Brocker C N, Yan T, Krausz K W, Xiang R, Gavrilova O, Patterson A D, Gonzalez F J. Intermittent fasting promotes white adipose browning and decreases obesity by shaping the gut microbiota. Cell Metabolism. 2017, 26(4): 672-685.e674

[14] Gasteiger G, Fan X, Dikiy S, Lee S Y, Rudensky A Y. Tissue residency of innate lymphoid cells in lymphoid and nonlymphoid organs. Science (New York, N.Y.). 2015, 350(6263): 981-985

[15] Vivier E, Artis D, Colonna M, Diefenbach A, Di Santo J P, Eberl G, Koyasu S, Locksley R M, McKenzie A N J, Mebius R E, Powrie F, Spits H. Innate lymphoid cells: 10 years on. Cell. 2018, 174(5): 1054-1066

[16] O'Sullivan T E, Rapp M, Fan X, Weizman O-E, Bhardwaj P, Adams N M, Walzer T, Dannenberg A J, Sun J C. Adipose-resident group 1 innate lymphoid cells promote obesity-associated insulin resistance. Immunity. 2016, 45(2): 428-441

[17] Wang H, Shen L, Sun X, Liu F, Feng W, Jiang C, Chu X, Ye X, Jiang C, Wang Y, Zhang P, Zang M, Zhu D, Bi Y. Adipose group 1 innate lymphoid cells promote adipose tissue fibrosis and diabetes in obesity. Nat Commun. 2019, 10(1): 3254

[18] Brestoff J R, Kim B S, Saenz S A, Stine R R, Monticelli L A, Sonnenberg G F, Thome J J, Farber D L, Lutfy K, Seale P, Artis D. Group 2 innate lymphoid cells promote beiging of white adipose tissue and limit obesity. Nature. 2015, 519(7542): 242-246

[19] Lee M W, Odegaard J I, Mukundan L, Qiu Y, Molofsky A B, Nussbaum J C, Yun K, Locksley R M, Chawla A. Activated type 2 innate lymphoid cells regulate beige fat biogenesis. Cell. 2015, 160(1-2): 74-87

[20] Wang L, Luo Y, Luo L, Wu D, Ding X, Zheng H, Wu H, Liu B, Yang X, Silva F, Wang C, Zhang X, Zheng X, Chen J, Brigman J, Mandell M, Zhou Z, Liu F, Yang X O, Liu M. Adiponectin restrains ILC2 activation by ampk-mediated feedback inhibition of IL-33 signaling. J Exp Med. 2021, 218(2):

[21] Sanos S L, Bui V L, Mortha A, Oberle K, Heners C, Johner C, Diefenbach A. Rorgammat and commensal microflora are required for the differentiation of mucosal interleukin 22-producing NKp46^{+} cells. Nature Immunology. 2009, 10(1): 83-91

[22] Wang X, Ota N, Manzanillo P, Kates L, Zavala-Solorio J, Eidenschenk C, Zhang J, Lesch J, Lee W P, Ross J, Diehl L, van Bruggen N, Kolumam G, Ouyang W. Interleukin-22 alleviates metabolic disorders and restores mucosal immunity in diabetes. Nature. 2014, 514(7521): 237-241

[23] Hasnain S Z, Borg D J, Harcourt B E, Tong H, Sheng Y H, Ng C P, Das I, Wang R, Chen A C H, Loudovaris T, Kay T W, Thomas H E, Whitehead J P, Forbes J M, Prins J B, McGuckin M A. Glycemic control in diabetes is restored by therapeutic manipulation of cytokines that regulate beta cell stress. Nature Medicine. 2014, 20(12): 1417-1426

[24] Qi X, Yun C, Sun L, Xia J, Wu Q, Wang Y, Wang L, Zhang Y, Liang X, Wang L, Gonzalez F J, Patterson A D, Liu H, Mu L, Zhou Z, Zhao Y, Li R, Liu P, Zhong C, Pang Y, Jiang C, Qiao J. Gut microbiota–bile acid–interleukin-22 axis orchestrates polycystic ovary syndrome. Nature Medicine. 2019, 25(8): 1225-1233

[25] Sasaki T, Moro K, Kubota T, Kubota N, Kato T, Ohno H, Nakae S, Saito H, Koyasu S. Innate lymphoid cells in the induction of obesity. Cell Reports. 2019, 28(1): 202-217.e207

[26] Upadhyay V, Poroyko V, Kim T J, Devkota S, Fu S, Liu D, Tumanov A V, Koroleva E P, Deng L, Nagler C, Chang E B, Tang H, Fu Y X. Lymphotoxin regulates commensal responses to enable diet-induced obesity. Nat Immunol. 2012, 13(10): 947-953

[27] Wang Y, Kuang Z, Yu X, Ruhn K A, Kubo M, Hooper L V. The intestinal microbiota regulates body composition through nfil3 and the circadian clock. Science. 2017, 357(6354): 912-916

[28] Kawano Y, Edwards M, Huang Y, Bilate A M, Araujo L P, Tanoue T, Atarashi K, Ladinsky M S, Reiner S L, Wang H H, Mucida D, Honda K, Ivanov, II. Microbiota imbalance induced by dietary sugar disrupts immune-mediated protection from metabolic syndrome. Cell. 2022, 185(19): 3501-3519.e3520

[29] Seillet C, Luong K, Tellier J, Jacquelot N, Shen R D, Hickey P, Wimmer V C, Whitehead L, Rogers K, Smyth G K, Garnham A L, Ritchie M E, Belz G T. The neuropeptide vip confers anticipatory mucosal immunity by regulating ILC3 activity. Nature Immunology. 2020, 21(2): 168-177

[30] Victor A R, Nalin A P, Dong W, McClory S, Wei M, Mao C, Kladney R D, Youssef Y, Chan W K, Briercheck E L, Hughes T, Scoville S D, Pitarresi J R, Chen C, Manz S, Wu L C, Zhang J, Ostrowski M C, Freud A G, Leone G W, Caligiuri M A, Yu J. Il-18 drives ILC3 proliferation and promotes IL-22 production via nf-κb. J Immunol. 2017, 199(7): 2333-2342

[31] Gronke K, Hernández P P, Zimmermann J, Klose C S N, Kofoed-Branzk M, Guendel F, Witkowski M, Tizian C, Amann L, Schumacher F, Glatt H, Triantafyllopoulou A, Diefenbach A. Interleukin-22 protects intestinal stem cells against genotoxic stress. Nature. 2019, 566(7743): 249-253

[32] Kim M H, Taparowsky E J, Kim C H. Retinoic acid differentially regulates the migration of innate lymphoid cell subsets to the gut. Immunity. 2015, 43(1): 107-119

[33] Mackley E C, Houston S, Marriott C L, Halford E E, Lucas B, Cerovic V, Filbey K J, Maizels R M, Hepworth M R, Sonnenberg G F, Milling S, Withers D R. Ccr7-dependent trafficking of rorγ^{+} ilcs creates a unique microenvironment within mucosal draining lymph nodes. Nat Commun. 2015, 6: 5862

[34] Yu H B, Yang H, Allaire J M, Ma C, Graef F A, Mortha A, Liang Q, Bosman E S, Reid G S, Waschek J A, Osborne L C, Sokol H, Vallance B A, Jacobson K. Vasoactive intestinal peptide promotes host defense against enteric pathogens by modulating the recruitment of group 3 innate lymphoid cells. Proc Natl Acad Sci U S A. 2021, 118(41):

[35] Zou J, Chassaing B, Singh V, Pellizzon M, Ricci M, Fythe M D, Kumar M V, Gewirtz A T. Fiber-mediated nourishment of gut microbiota protects against diet-induced obesity by restoring IL-22-mediated colonic health. Cell Host Microbe. 2018, 23(1): 41-53.e44

[36] Qi X, Yun C, Sun L, Xia J, Wu Q, Wang Y, Wang L, Zhang Y, Liang X, Wang L, Gonzalez F J, Patterson A D, Liu H, Mu L, Zhou Z, Zhao Y, Li R, Liu P, Zhong C, Pang Y, Jiang C, Qiao J. Gut microbiota-bile acid-interleukin-22 axis orchestrates polycystic ovary syndrome. Nat Med. 2019, 25(8): 1225-1233

[37] Li H, Dong M, Liu W, Gao C, Jia Y, Zhang X, Xiao X, Liu Q, Lin H. Peripheral IL-6/stat3 signaling promotes beiging of white fat. Biochim Biophys Acta Mol Cell Res. 2021, 1868(10): 119080

[38] Zhang Y, Xie C, Wang H, Foss R M, Clare M, George E V, Li S, Katz A, Cheng H, Ding Y, Tang D, Reeves W H, Yang L J. Irisin exerts dual effects on browning and adipogenesis of human white adipocytes. Am J Physiol Endocrinol Metab. 2016, 311(2): E530-541

[39] Talbot J, Hahn P, Kroehling L, Nguyen H, Li D, Littman D R. Feeding-dependent vip neuron-ILC3 circuit regulates the intestinal barrier. Nature. 2020, 579(7800): 575-580

[40] Yu H B, Yang H, Allaire J M, Ma C, Graef F A, Mortha A, Liang Q, Bosman E S, Reid G S, Waschek J A, Osborne L C, Sokol H, Vallance B A, Jacobson K. Vasoactive intestinal peptide promotes host defense against enteric pathogens by modulating the recruitment of group 3 innate lymphoid cells. Proceedings of the National Academy of Sciences of the United States of America. 2021, 118(41): e2106634118

[41] Stockinger B, Di Meglio P, Gialitakis M, Duarte J H. The aryl hydrocarbon receptor: Multitasking in the immune system. Annu Rev Immunol. 2014, 32: 403-432

[42] Ibiza S, García-Cassani B, Ribeiro H, Carvalho T, Almeida L, Marques R, Misic A M, Bartow-McKenney C, Larson D M, Pavan W J, Eberl G, Grice E A, Veiga-Fernandes H. Glial-cell-derived neuroregulators control type 3 innate lymphoid cells and gut defence. Nature. 2016, 535(7612): 440-443

[43] Chen H, Sun L, Feng L, Mulholland M, Zhang W, Yin Y. Peptidoglycan inhibits beigeing of adipose tissue. Acta Pharm Sin B. 2022, 12(2): 990-993

[44] Hildreth A D, Ma F, Wong Y Y, Sun R, Pellegrini M, O'Sullivan T E. Single-cell sequencing of human white adipose tissue identifies new cell states in health and obesity. Nature Immunology. 2021, 22(5): 639-653

[45] Hu B, Jin C, Zeng X, Resch J M, Jedrychowski M P, Yang Z, Desai B N, Banks A S, Lowell B B, Mathis D, Spiegelman B M. γδ T cells and adipocyte il-17rc control fat innervation and thermogenesis. Nature. 2020, 578(7796): 610-614

[46] Wang Q, Li D, Cao G, Shi Q, Zhu J, Zhang M, Cheng H, Wen Q, Xu H, Zhu L, Zhang H, Perry R J, Spadaro O, Yang Y, He S, Chen Y, Wang B, Li G, Liu Z, Yang C, Wu X, Zhou L, Zhou Q, Ju Z, Lu H, Xin Y, Yang X, Wang C, Liu Y, Shulman G I, Dixit V D, Lu L, Yang H, Flavell R A, Yin Z. Il-27 signalling promotes adipocyte thermogenesis and energy expenditure. Nature. 2021, 600(7888): 314-318

[47] Brooks J F, Behrendt C L, Ruhn K A, Lee S, Raj P, Takahashi J S, Hooper L V. The microbiota coordinates diurnal rhythms in innate immunity with the circadian clock. Cell. 2021, 184(16): 4154–4167.e4112

[48] Aune U L, Ruiz L, Kajimura S. Isolation and differentiation of stromal vascular cells to beige/brite cells. J Vis Exp. 2013, (73): 50191

[49] Seale P, Conroe H M, Estall J, Kajimura S, Frontini A, Ishibashi J, Cohen P, Cinti S, Spiegelman B M. Prdm16 determines the thermogenic program of subcutaneous white adipose tissue in mice. The Journal of Clinical Investigation. 2011, 121(1): 96-105

Figure and Figure Legends

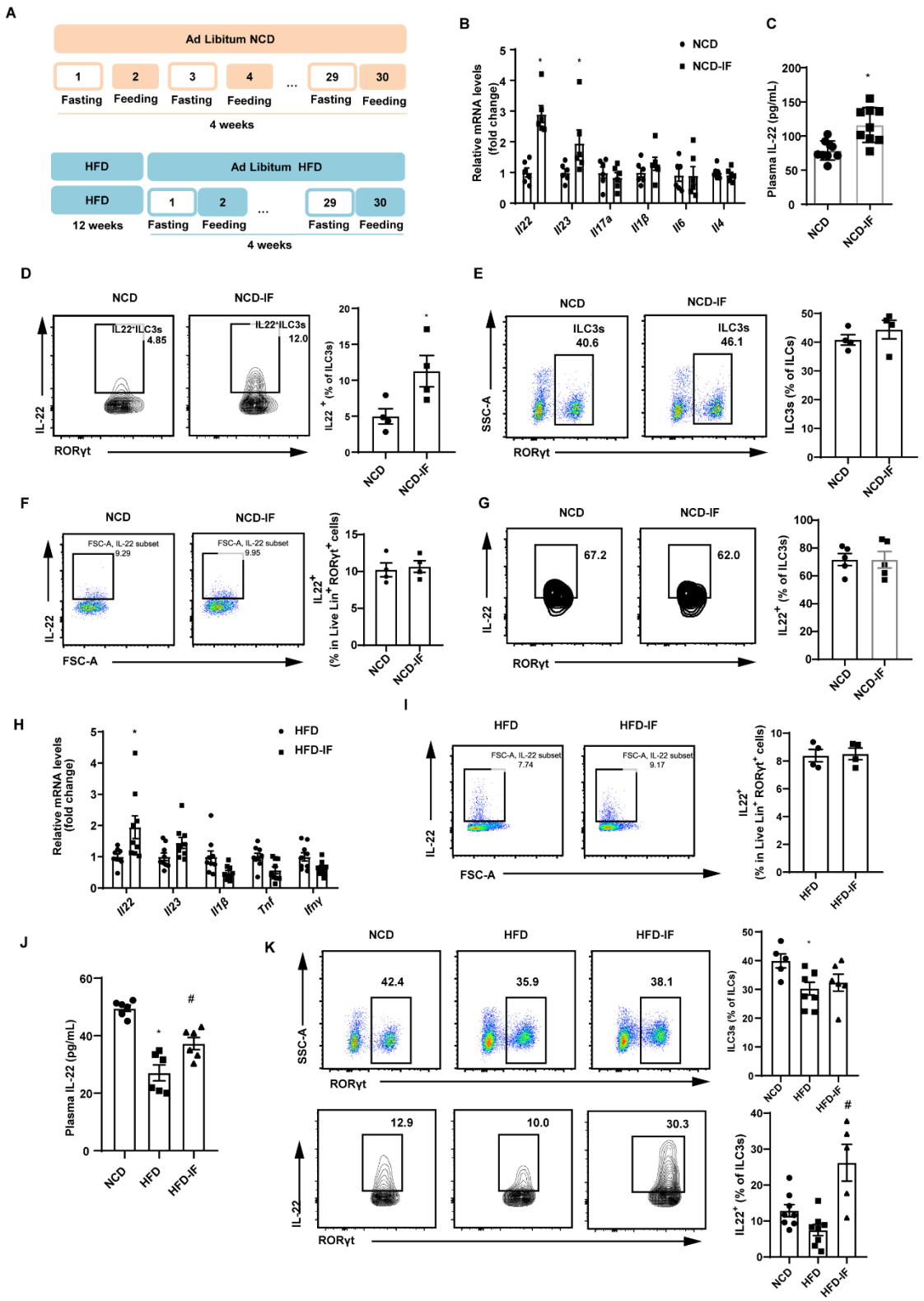

696

697 **Fig. 1. Intermittent fasting enhances IL-22 production by intestinal ILC3s.**

698 A Schematic illustration of the alternate day fasting regimen. NCD, normal chow diet.

699 HFD, high-fat diet. We applied alternate-day fasting to mice fed normal chow diet

700 (NCD-IF group) or high-fat diet (HFD-IF group). The control groups were at free access
701 to NCD (NCD group) or HFD (HFD group). n = 9 for each group.
702 B mRNA expression levels of cytokine genes in the small intestine of NCD and NCD
703 intermittent fasting (NCD-IF) mice. qPCR results were normalized to β-actin. n=6 for
704 each group.
705 C Protein levels of IL-22 in plasma of NCD and NCD intermittent fasting (NCD-IF)
706 mice. n=9 for each group.
707 D Flow cytometric analysis of IL-22^{+} cells in live CD127^{+} lineage^{-} RORγt^{+} ILC3s from
708 the small intestine lamina propria (siLP) of NCD and NCD intermittent fasting (NCD-
709 IF) mice. Four independent experiments were performed with similar results. n = 4.
710 E Flow cytometric analysis of RORγt^{+} ILC3s in live CD127^{+} lineage^{-} ILCs in the small
711 intestine lamina propria of NCD and NCD intermittent fasting (NCD-IF) mice. n = 4.
712 F Flow cytometric analysis of IL-22^{+} cells in Live Lineage^{+} RORγt^{+} cells in the small
713 intestine lamina propria of mice fed NCD with or without intermittent fasting. n = 4.
714 G Flow cytometric analysis of IL-22^{+} cells in CD90.2^{+} Lineage^{-} RORγt^{+} ILC3s from
715 the SVF cells of sWAT in mice fed NCD with or without intermittent fasting. n= 5.
716 H mRNA expression levels of cytokine genes in the small intestine of mice fed HFD
717 with or without intermittent fasting. qPCR results were normalized to β–actin. n= 9.
718 I Flow cytometric analysis of IL-22^{+} cells in Live Lineage^{+} RORγt^{+} cells in the small
719 intestine lamina propria of mice fed HFD with or without intermittent fasting. n=4.
720 J Levels of IL-22 in plasma of NCD mice, HFD mice and HFD-IF mice. n=6.
721 K Flow cytometric analysis of RORγt^{+} ILC3s in live CD127^{+} lineage^{-} ILCs and flow

722 cytometric analysis of IL-22^{+} cells in live CD127^{+} lineage^{-} RORγt^{+} ILC3s from the
723 small intestine lamina propria of NCD mice, HFD mice and HFD-IF mice. n=5-8. * vs
724 NCD, # vs HFD, $P < 0.05$.
725 All data represent the mean ± s.e.m. Statistical significance was determined by unpaired
726 two-tailed Student's *t* test (A-I) or one-way ANOVA with Bonferroni's multiple-
727 comparisons test (J-K). NCD, normal chow diet. HFD, high-fat diet. NCD-IF, normal
728 chow diet with intermittent fasting. HFD-IF, high-fat diet with intermittent fasting.
729

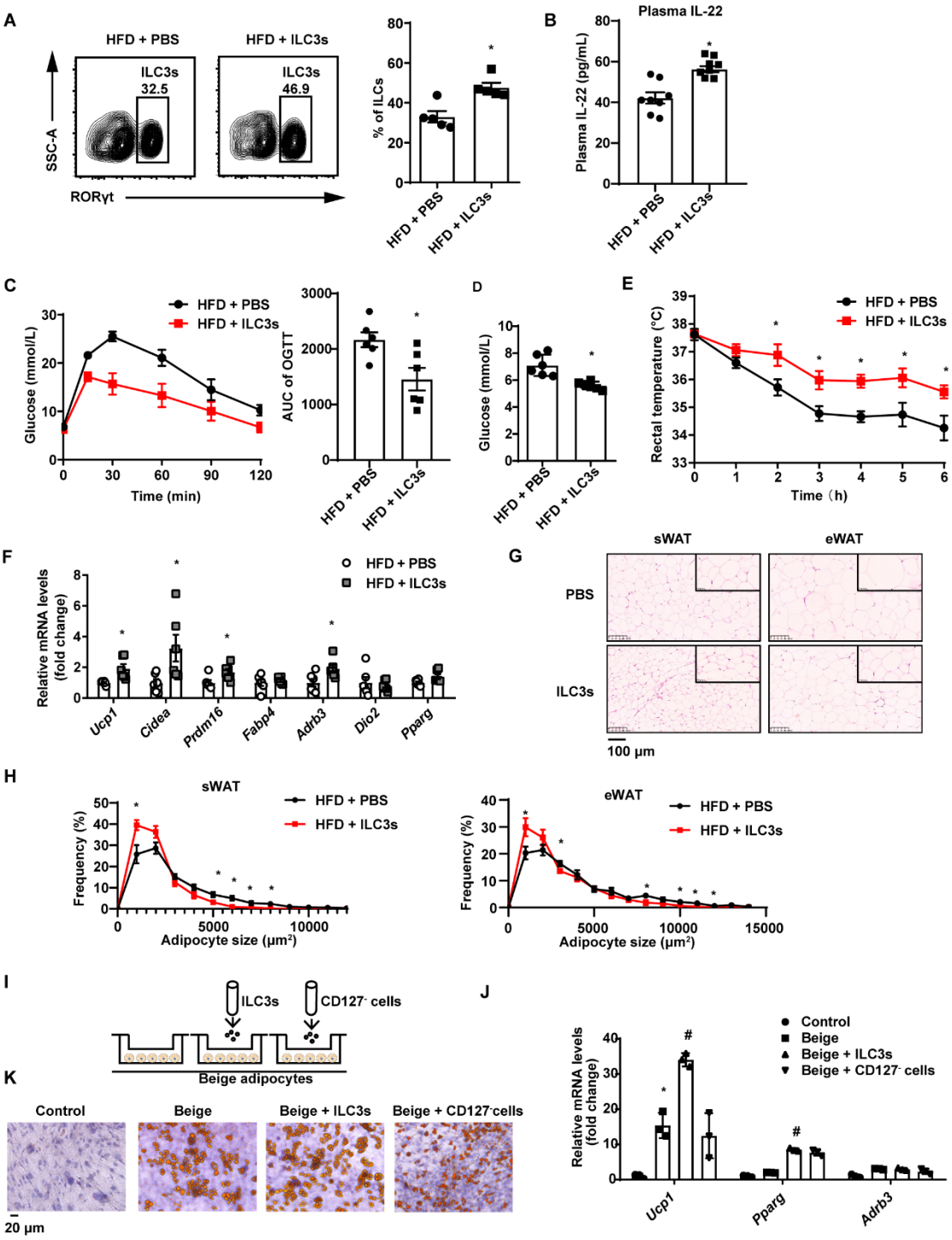

Fig. 2. ILC3s promote beigeing of white adipose tissue.

6 weeks old male C57BL/6J SPF wild type mice were fed with HFD for 16 weeks and then injected with ILC3s (HFD + ILC3s group) or PBS (HFD + PBS group) intravenously six times in a month. n=8 for each group.

A. Flow cytometric analysis of RORγt^{+} ILC3s in live CD127^{+} lineage^{-} ILCs from the

736 siLP of mice transferred with PBS or ILC3s. The proportion of ILC3s in ILCs was
737 shown in the histogram. n=5 for each group.
738 B. Levels of IL-22 in plasma. n=8 for each group.
739 C. Oral glucose tolerance test (OGTT) and area under the curve (AUC). n=6 mice/group.
740 D. Random blood glucose. n=6 mice/group.
741 E. Rectal temperature of HFD mice transferred with PBS or ILC3s during a 6 h cold
742 challenge (4 °C). n=6 mice/group.
743 F. qPCR analysis of thermogenic genes in sWAT. n=6 mice/group.
744 G. Representative images of hematoxylin-and-eosin-stained sections of sWAT, eWAT
745 and BAT from HFD mice transferred with ILC3s or control (n=5).
746 H. Distribution and average adipocyte size of sWAT and eWAT were shown (n=5).
747 I. Schematic depicting the coculture of ILC3s with SVF-derived beige adipocytes.
748 J. qPCR analysis of thermogenic genes in SVF-derived cells. * indicates P<0.05 vs
749 Control, # denotes P<0.05vs Beige. n=3.
750 K. Oil red O staining of adipocytes after coculture with ILC3s or $CD127^-$ cells.
751 All data represent the means ± SEM. Statistical significance was determined by
752 unpaired two-tailed Student's *t* test (A-H), one-way ANOVA with Bonferroni's
753 multiple-comparisons test (J).

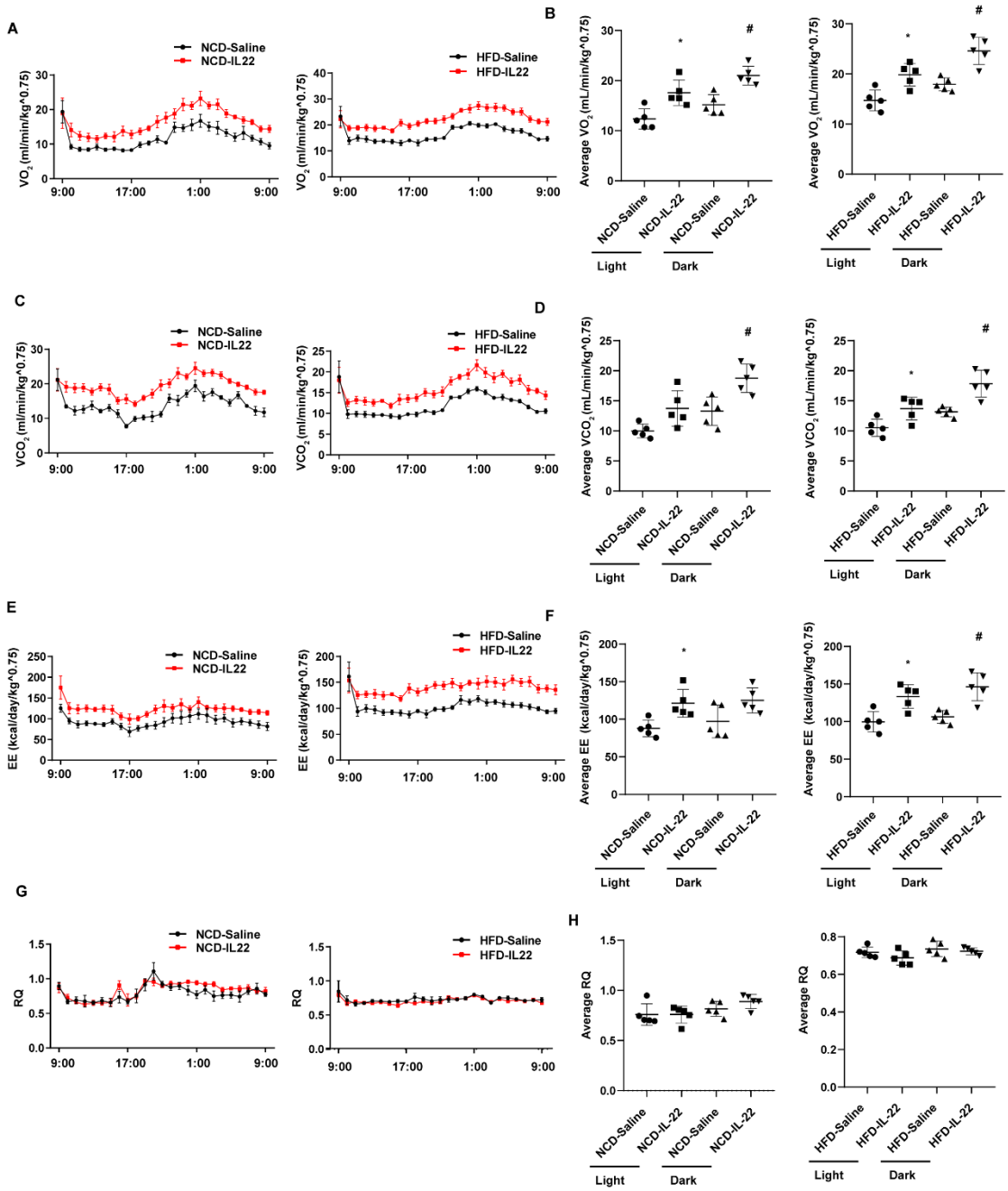

Fig.3. IL-22 promotes energy expenditure.

6 weeks old male C57BL/6J SPF wild type mice were fed NCD or HFD for 12 weeks and then divided into four groups (NCD-Saline, NCD-IL-22, HFD-Saline, HFD-IL-22). Mice were intraperitoneally injected with 4 μg/kg IL-22 every other day for six weeks. The control groups were injected with saline.

761 A VO_2 of mice fed NCD or HFD.

762 B. Average VO_2 at light and dark respectively.

763 C. VCO_2 of mice fed NCD or HFD.

764 D. Average VCO_2 at light and dark respectively.

765 E. Energy expenditure of mice fed NCD or HFD.

766 F. Average energy expenditure at light and dark respectively.

767 G. Respiratory quotient (RQ) of mice fed NCD or HFD

768 H. Average respiratory quotient at light and dark respectively.

769 * indicates $P<0.05$ vs NCD-Saline or HFD-Saline at light. # indicates $P<0.05$ vs NCD-

770 Saline or HFD-Saline at dark. n = 5. Statistical significance was determined by one-

771 way ANOVA with Bonferroni's multiple-comparisons test (B, D, F, H).

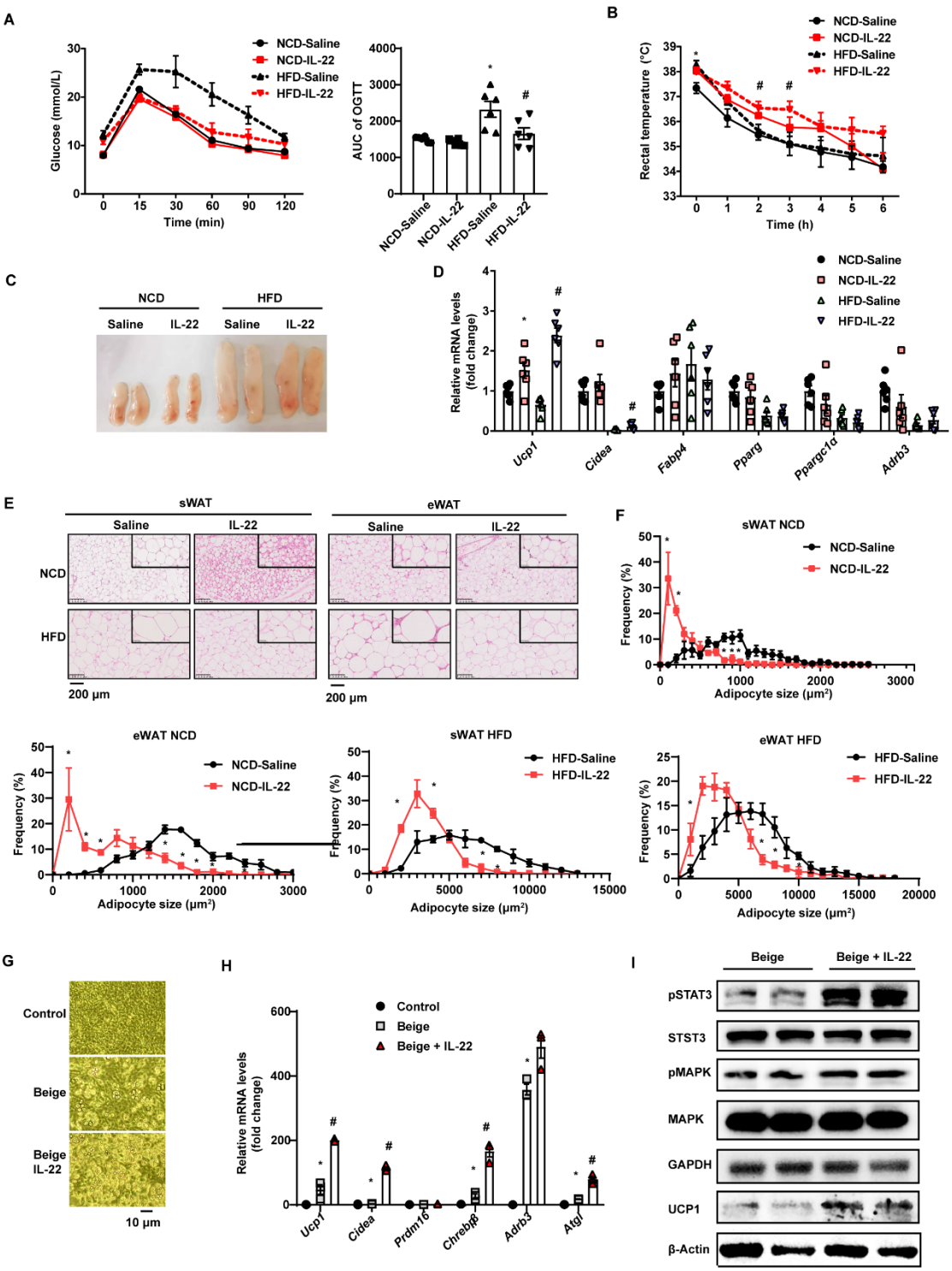

Fig. 4. IL-22 promotes beigeing of white adipose tissue.

6 weeks old male C57BL/6J SPF wild type mice were fed NCD or HFD for 12 weeks and then divided into four groups (NCD-Saline, NCD-IL-22, HFD-Saline, HFD-IL-22). Mice were intraperitoneally injected with 4 μg/kg IL-22 every other day for 6 weeks.

777 The saline group was injected with saline. n=6 mice/group.

778 A. Oral glucose tolerance test (OGTT) and area under the curve (AUC). n=6 mice/group.

779 * indicates P<0.05 vs NCD-Saline; # denotes P<0.05 vs HFD-Saline.

780 B. Rectal temperature of mice during a 6 h cold challenge (4 °C). n=6. * indicates

781 P<0.05 vs NCD-Saline; # denotes P<0.05 vs HFD-Saline.

782 C. Representative image of sWAT of the four groups, NCD-Saline, NCD-IL-22, HFD-

783 Saline, HFD-IL-22.

784 D. qPCR analysis of thermogenic genes of sWAT. n=6 mice/group. * indicates P<0.05

785 vs NCD-Saline; # denotes P<0.05 vs HFD-Saline.

786 E. Representative images of hematoxylin-and-eosin-stained sections of sWAT and

787 eWAT (n=5 for each group).

788 F. The distribution and average adipocyte size of sWAT and eWAT were determined by

789 ImageJ.

790 G. Phase-contrast microscopic images of SVF cells and adipocytes.

791 H. qPCR analysis of thermogenic genes in SVF cells and beige adipocytes. n=3. #

792 denotes P<0.05 vs Beige.

793 I. pSTAT3, STAT3, pMAPK, MAPK, GAPDH, UCP1, β-Actin protein expression in

794 the beige adipocytes or beige adipocytes treated with IL-22 detected by Western

795 blotting. GAPDH and β-Actin was used as the loading control.

796 All data represent the mean ± s.e.m. Statistical significance was determined by one-

797 way ANOVA with Bonferroni's multiple-comparisons test (A-D, H) or two-tailed

798 Student's *t* test (F). sWAT, subcutaneous white adipose tissue; eWAT, epididymal white

adipose tissue.

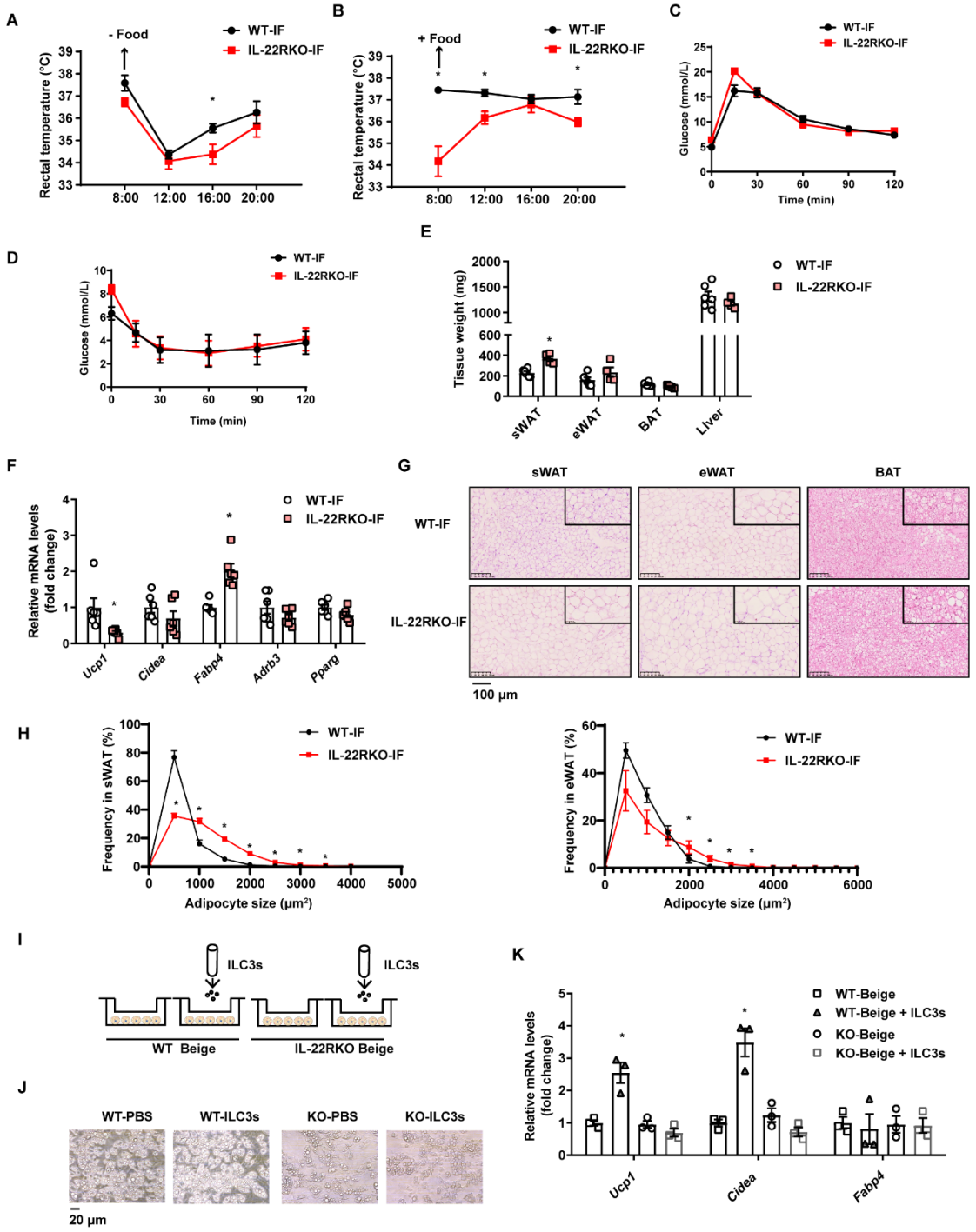

Fig. 5. IL-22RKO blocks white adipose tissue beigeing induced by intermittent fasting.

8 weeks old IL-22RKO and wild type mice were subjected to alternate day fasting for 30 days. n =6 mice per group.

805 A. Rectal temperature of mice at room temperature during the fasting day. n=6 per
806 group.
807 B. Rectal temperature of mice at room temperature during the fed day. n=6 per group.
808 C. Oral glucose tolerance test (OGTT) of WT-IF mice and IL-22RKO-IF mice. n=6 per
809 group.
810 D. Insulin tolerance test (ITT) of WT-IF mice and IL-22RKO-IF mice. n=6 per group.
811 E. Tissue weight of sWAT, eWAT, BAT, and liver from WT-IF and IL-22RKO-IF mice.
812 n=6 mice/group.
813 F. qPCR analysis of thermogenic genes in sWAT from WT-IF and IL-22RKO-IF mice.
814 n=6 mice/group.
815 G. Representative images of hematoxylin-and-eosin-stained sections of sWAT, eWAT
816 and BAT (n=5 for each group).
817 H. The distribution and average adipocyte size of sWAT and eWAT were determined by
818 ImageJ.
819 I. Schematic depicting the co-culture of ILC3s with SVF-induced beige adipocytes
820 from WT or IL-22RKO mice. n=3. Experiments were repeated 3 times.
821 J. Phase contrast microscopy images of beige adipocytes differentiated from SVF cells
822 cocultured with or without ILC3s. Shown are representatives from one experiment.
823 K. qPCR analysis of thermogenic genes in SVF-derived cells co-cultured with or
824 without ILC3s. n=3.
825 All data represent the means ± SEM. Statistical significance was determined by
826 unpaired two-tailed Student's *t* test (A-H) or one-way ANOVA with Bonferroni's

827 multiple-comparisons test (K).

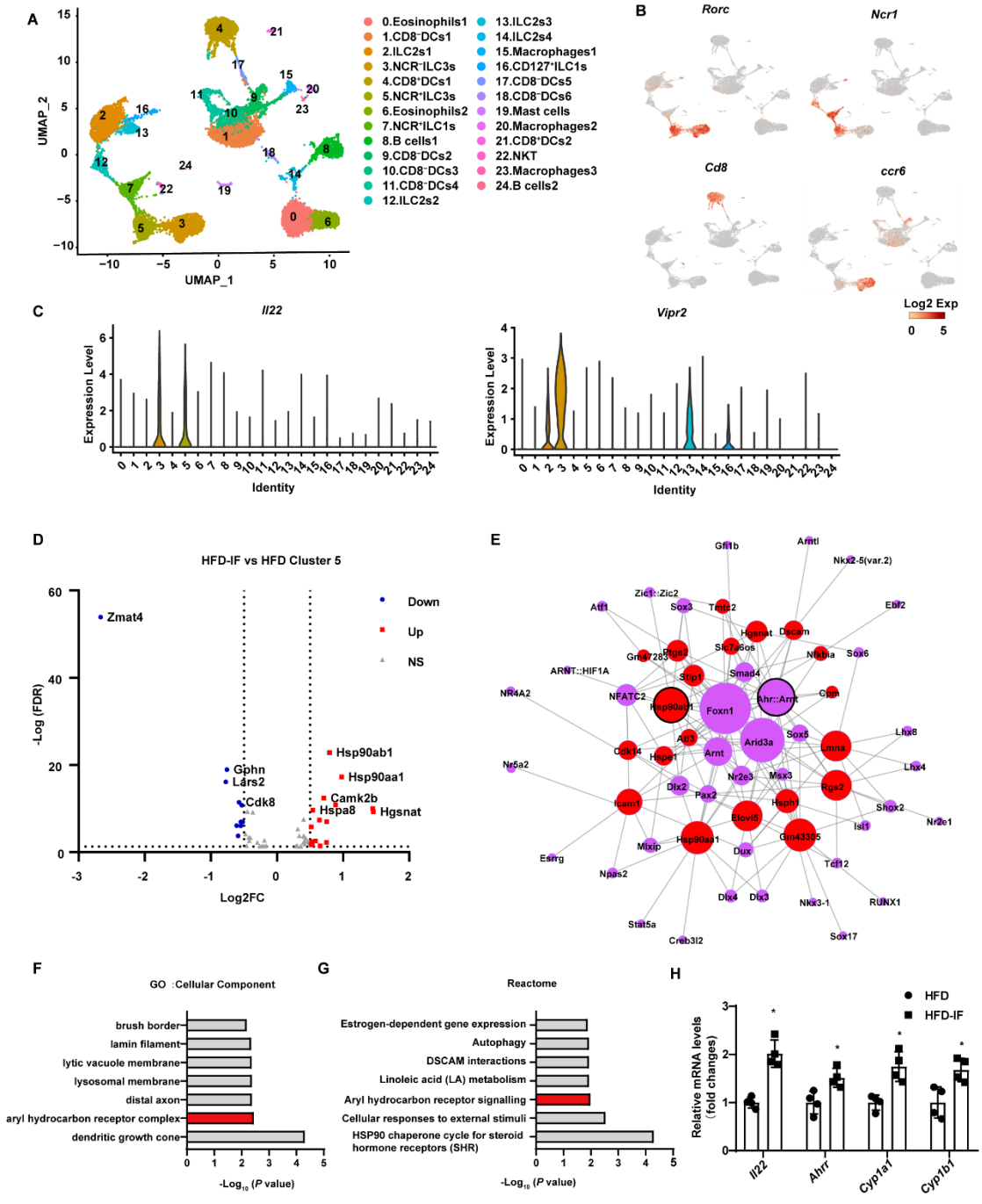

828

829 **Fig. 6. Profiling of intestinal immune cells derived from mice fed NCD, HFD and**

830 **HFD-IF.**

831 Live CD45+ Lineage -Cells sorted from mice fed normal chow diet (NCD group), high-

832 fat diet (HFD- group), high-fat diet with alternate day fasting (HFD-IF group) were

833 analyzed using single cell sequencing.

834 A. Cell subsets in the small intestine lamina propria $CD45^+$ $Lineage^-$ immune cell atlas.
835 Two-dimensional (2D) representation of cell profiles (dots) from the small intestine
836 lamina propria, colored and numbered by cluster membership.
837 B-C. UMAP feature plots (B) and violin plots (C) showing RNA expression of cluster
838 markers for the indicated cell populations. UMAP feature plots are based on the UMAP
839 shown in Figure 6A.
840 D. The volcano plot of differentially expressed genes in Cluster 5 (NCR^+ ILC3s). The
841 red dots represent upregulated genes in HFD-IF group compared with HFD group,
842 while the blue dots represent downregulated genes in HFD-IF group compared with
843 HFD group. Hsp90ab1 is one of the notably upregulated genes.
844 E. Transcription factor prediction using the Jaspar database and TFBS tools. Red dots
845 represent differentially expressed genes, purple dots represent transcription factors, and
846 larger nodes represent more nodes connected to them.
847 F. Gene ontology (GO) of the top 20 differentially expressed genes in Cluster 5. The
848 cellular component up GO terms in HFD-IF group compared with HFD group.
849 G. The reactome up terms of Cluster 5 top 20 differential genes in HFD-IF group
850 compared with HFD group.
851 H. qPCR analysis of AHR target genes in ILC3s sorted from HFD and HFD-IF mice.
852 n=4. *, $P<0.05$, All data represent the means ± SEM. Statistical significance was
853 determined by unpaired two-tailed Student's *t* test.
854

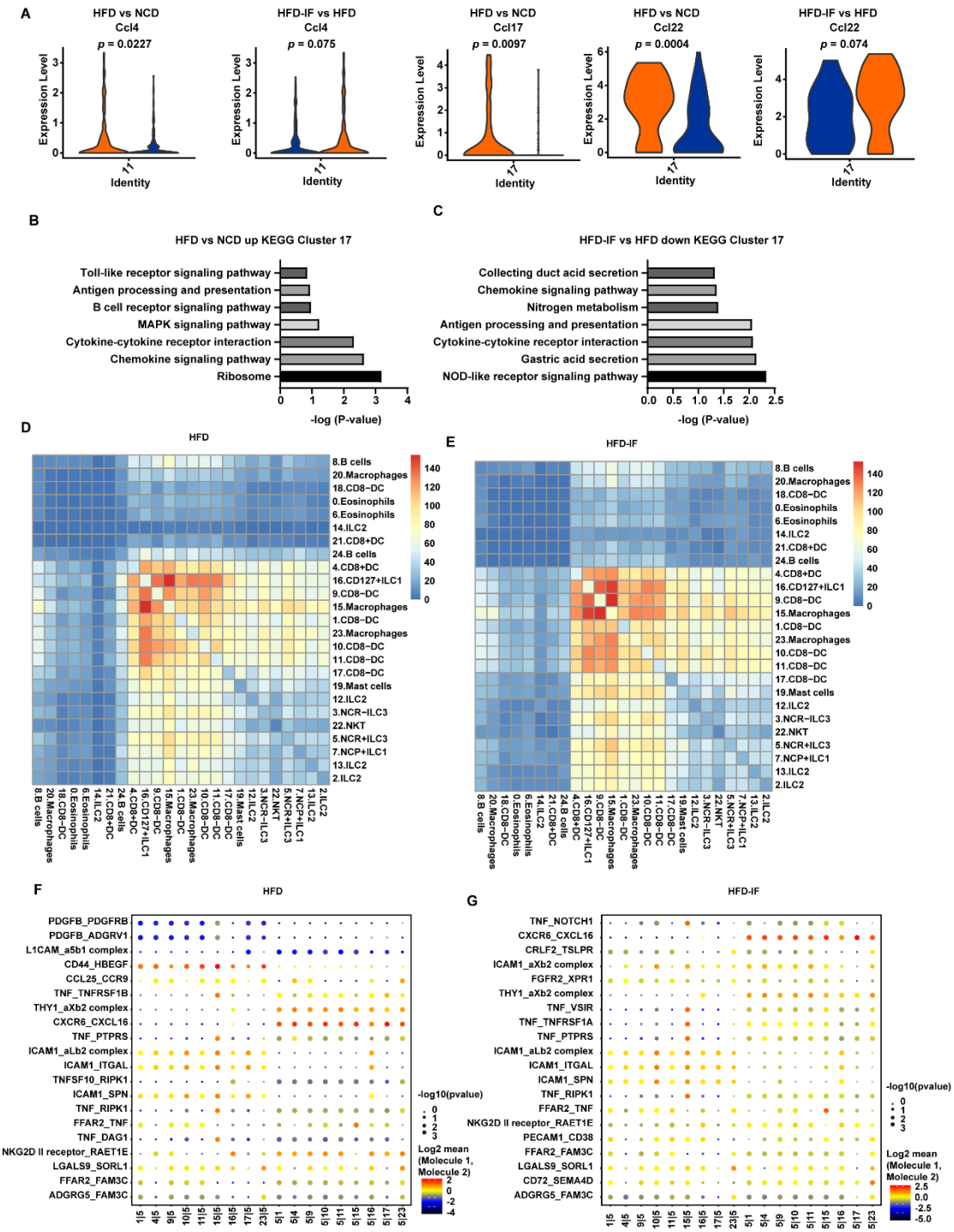

Fig. 7. Interaction between myeloid cells and ILC3s.

A. Violin plots showing the RNA expression of chemokines in CD8$^-$DCs (cluster 11 and cluster 17).

B. KEGG enrichment in upregulated genes of CD8$^-$DCs of HFD group compared with NCD group (cluster 17).

861 C. KEGG enrichment of downregulated genes of $CD8^-$DCs of HFD-IF group compared
862 with HFD group (cluster 17).
863 D. Heatmap showing the number of significant interactions identified between cell
864 types in sorted siLP immune cells of HFD mice as determined by Cellphone DB. The
865 color represents the number of interactions between cell types, a higher number of
866 interactions (red) and a lower number of interactions (blue).
867 E. Heatmap showing the number of significant interactions identified between cell
868 types in sorted siLP immune cells of HFD-IF mice as determined by Cellphone DB.
869 The color represents the number of interactions between cell types: a higher number of
870 interactions (red) and a lower number of interactions (blue).
871 F. Interaction pattern of the top 20 protein pairs and the top 20 cell types in sorted siLP
872 immune cells of HFD group mice. The x-axis is the cell type interaction, and the y-axis
873 is the protein interaction. The larger the point is, the smaller the p value. The color
874 represents the average expression, and red to black indicates the level from high to low.
875 G. Interaction pattern of the top 20 protein pairs and the top 20 cell types in sorted siLP
876 immune cells of HFD-IF mice. The x-axis is the cell type interaction, and the y-axis is
877 the protein interaction. The larger the point is, the smaller the p value. The color
878 represents the average expression, and red to black indicates the level from high to low.

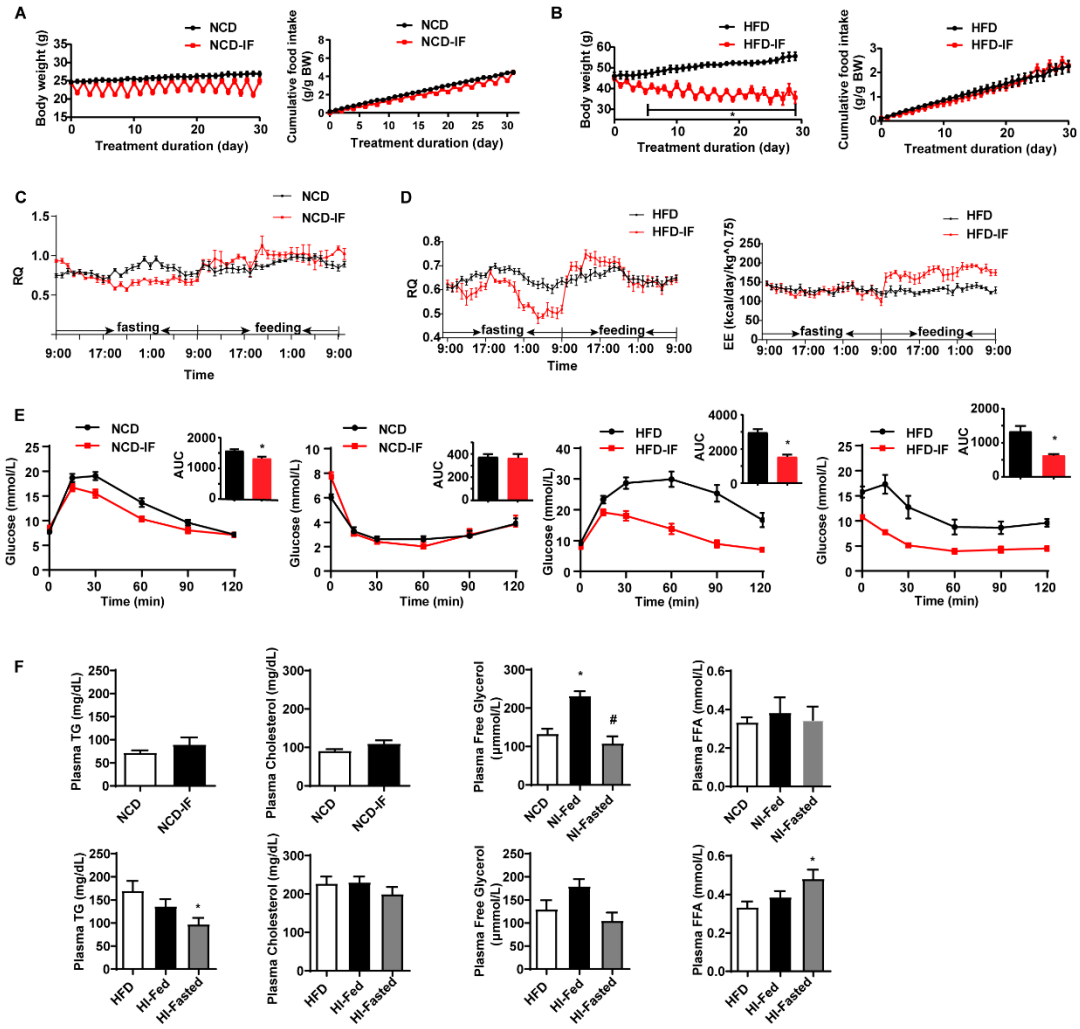

Supplementary Figure 1 Intermittent fasting improves glucose metabolism and lipid metabolism.

A. Body weight and cumulative food intake normalized to body weight of mice fed NCD with or without intermittent fasting. n=9.

B. Body weight and cumulative food intake normalized to body weight of mice fed HFD with or without intermittent fasting. n=9.

C. Respiratory quotient (RQ) of mice fed NCD with or without intermittent fasting. n=5.

D. Respiratory quotient (RQ), energy expenditure (EE) of mice fed HFD with or without intermittent fasting. n=5.

E. Oral glucose tolerance test (OGTT) and area under the curve (AUC). Insulin tolerance test (ITT) and area under the curve (AUC) of NCD, NCD-IF, HFD and HFD-IF mice. n=6 per group.

F. Levels of plasma triglycerides (TG), cholesterol, free glycerol and free fatty acids (FFA). n=6 mice/group.

All data represent the mean ± s.e.m. Statistical significance was determined by unpaired two-tailed Student's *t* test or one-way ANOVA with Bonferroni's multiple-comparisons test.

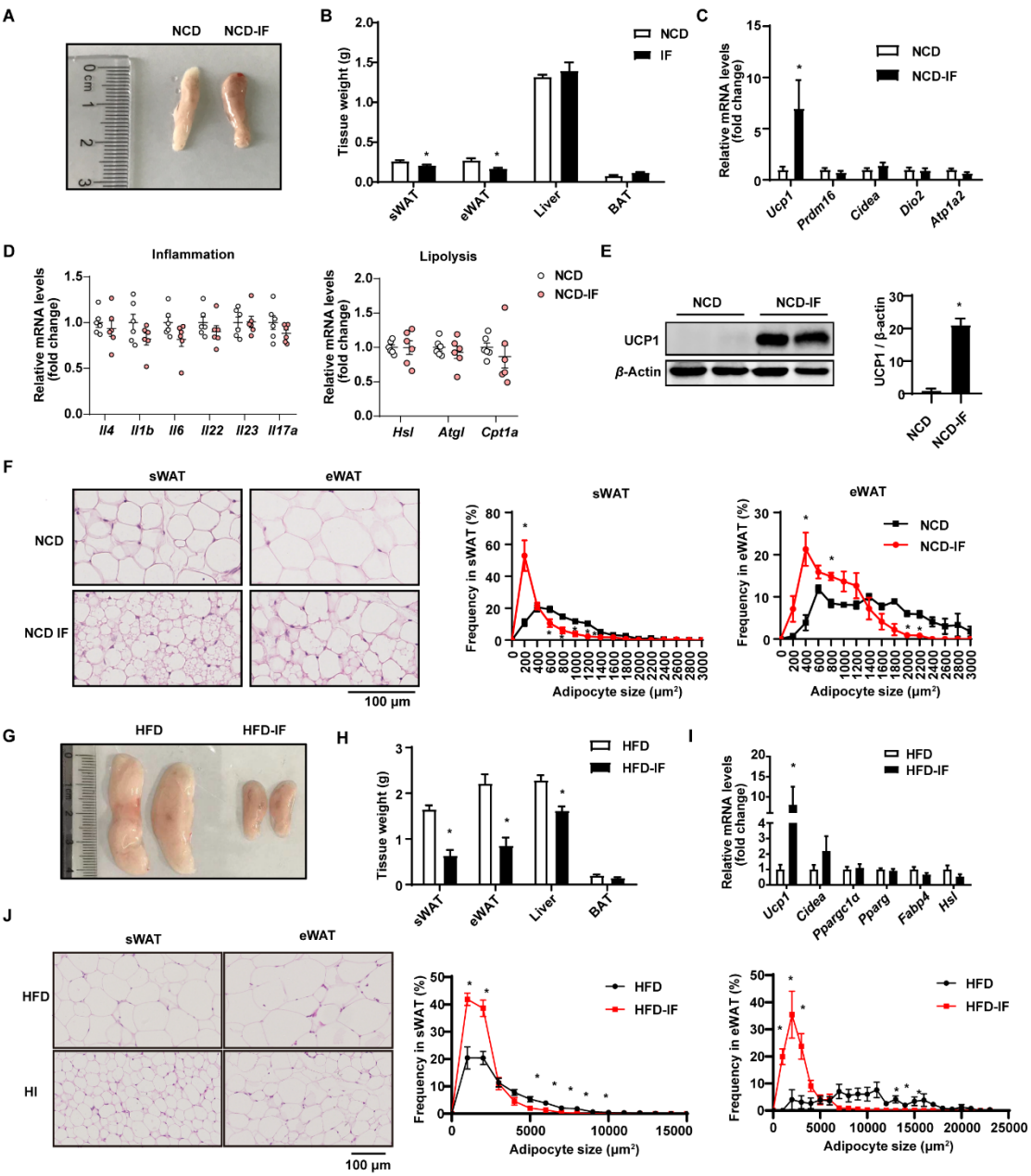

Supplementary Figure 2 Intermittent fasting promotes white adipose tissue beigeing.

A. Representative image of sWAT from mice fed NCD with or without intermittent fasting.

B. Tissue weight of sWAT, eWAT, Liver, BAT, from NCD and NCD-IF mice. n=6.

C. qPCR analysis of thermogenic genes in sWAT from NCD and NCD-IF mice. n=6 mice/group.

906 D. qPCR analysis of inflammation and lipolysis genes in sWAT from NCD and NCD-
907 IF mice. n=6 mice/group.
908 E. UCP1 protein expression in the sWAT of NCD and NCD IF mice detected by Western
909 blotting. β-actin was used as the loading control. The relative protein signal intensity
910 was quantified using ImageJ software.
911 F. H&E staining in sWAT and eWAT. Cell sizes were measured using ImageJ. n=5 per
912 group. Scale bar: 100 μm.
913 G.Representative image for sWAT of HFD and HFD-IF mice. n=6.
914 H. Tissue weight of sWAT, BAT, Liver, eWAT from HFD and HFD-IF mice. n=6.
915 I. qPCR analysis of thermogenic genes in sWAT from HFD and HFD-IF mice. n=6
916 mice/group.
917 J. H&E staining in sWAT and eWAT from HFD and HFD-IF mice. Cell sizes were
918 measured using ImageJ. n=5 per group. Scale bar: 100 μm.
919 All data represent the mean ± s.e.m. Statistical significance was determined by unpaired
920 two-tailed Student's *t* test (B-E, H, I).

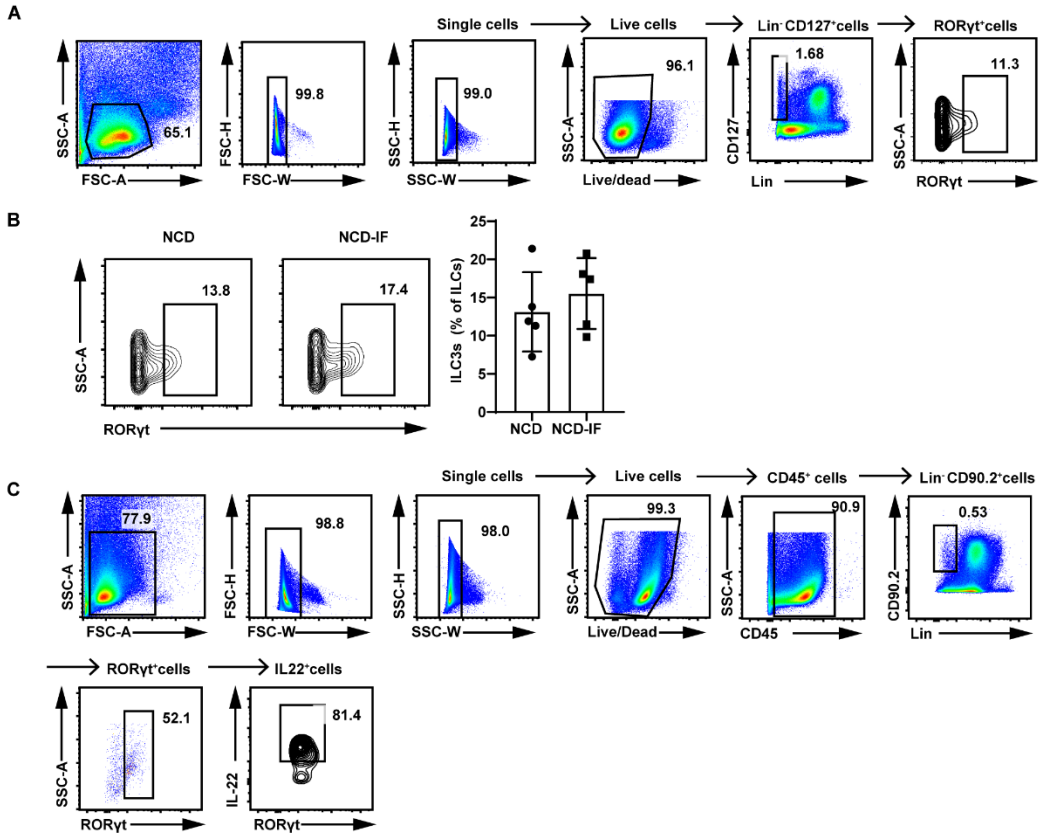

Supplementary Figure 3 Intermittent fasting demonstrates no effect on the number of ILC3s in sWAT.

A. Gating strategy for flow cytometry analysis of live lineage^{-}CD127^{+}RORγt^{+}ILC3s in the SVF of sWAT.

B. Flow cytometric analysis of RORγt^{+} ILC3s in live CD127^{+} lineage^{-} ILCs from the sWAT of NCD mice, NCD-IF mice. n=5.

C. Gating strategy for flow cytometry analysis of IL-22^{+} cells in live CD45^{+}lineage^{-}CD90.2^{+}RORγt^{+}ILC3s in the SVF of sWAT.

All data represent the mean ± s.e.m. Statistical significance was determined by unpaired two-tailed Student's *t* test.

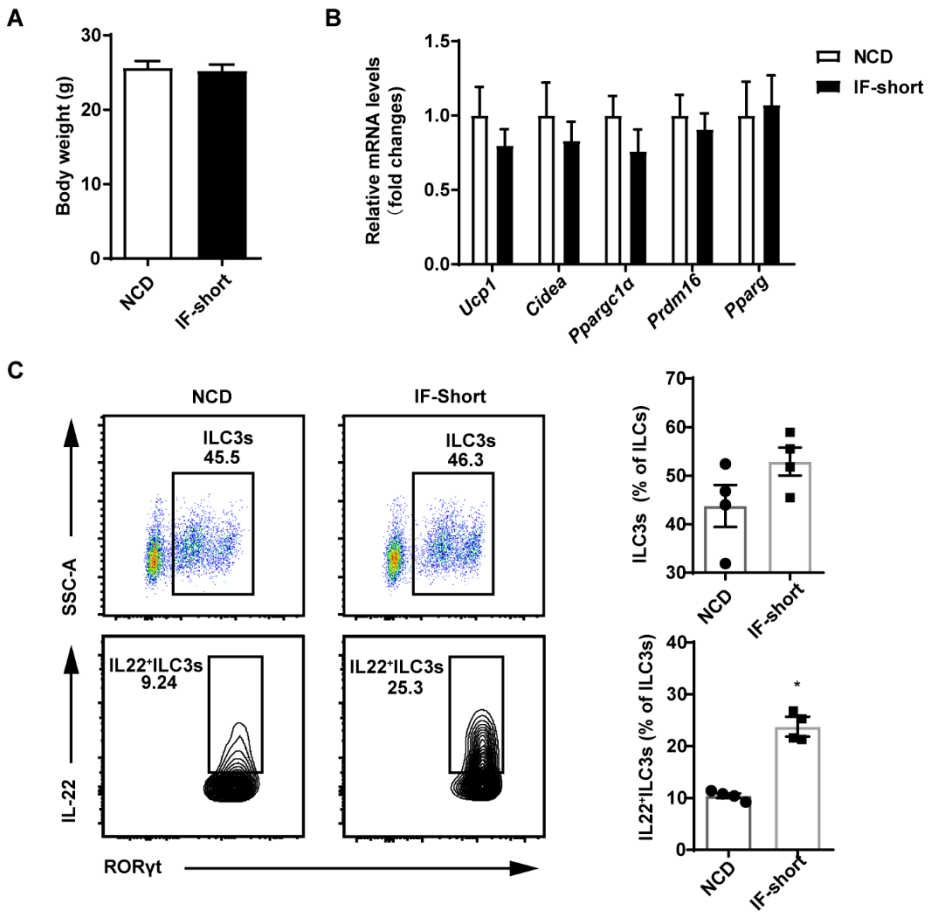

Supplementary Figure 4 Short-term intermittent fasting induces intestinal ILC3s to secrete IL-22.

Eight-week-old SPF mice were exposed to one cycle of intermittent fasting for 2 days (IF-short), while the control group (NCD) has free access to NCD. n=6.

A. Body weight of NCD and IF-short mice. n=6.

B. qPCR analysis of thermogenic genes in sWAT from NCD and IF-short mice. n=6 mice/group.

C. Flow cytometric analysis of RORγt^{+} ILC3s in live CD127^{+} lineage^{-} ILCs in the small intestine lamina propria of NCD or IF-short mice. Flow cytometric analysis of IL-22^{+} cells in live CD127^{+} lineage^{-} RORγt^{+} ILC3s from the small intestine lamina propria of

943 NCD or IF-short mice. Four independent experiments were performed with similar

944 results. n=4.

945 All data represent the mean ± s.e.m. Statistical significance was determined by unpaired

946 two-tailed Student's *t* test.

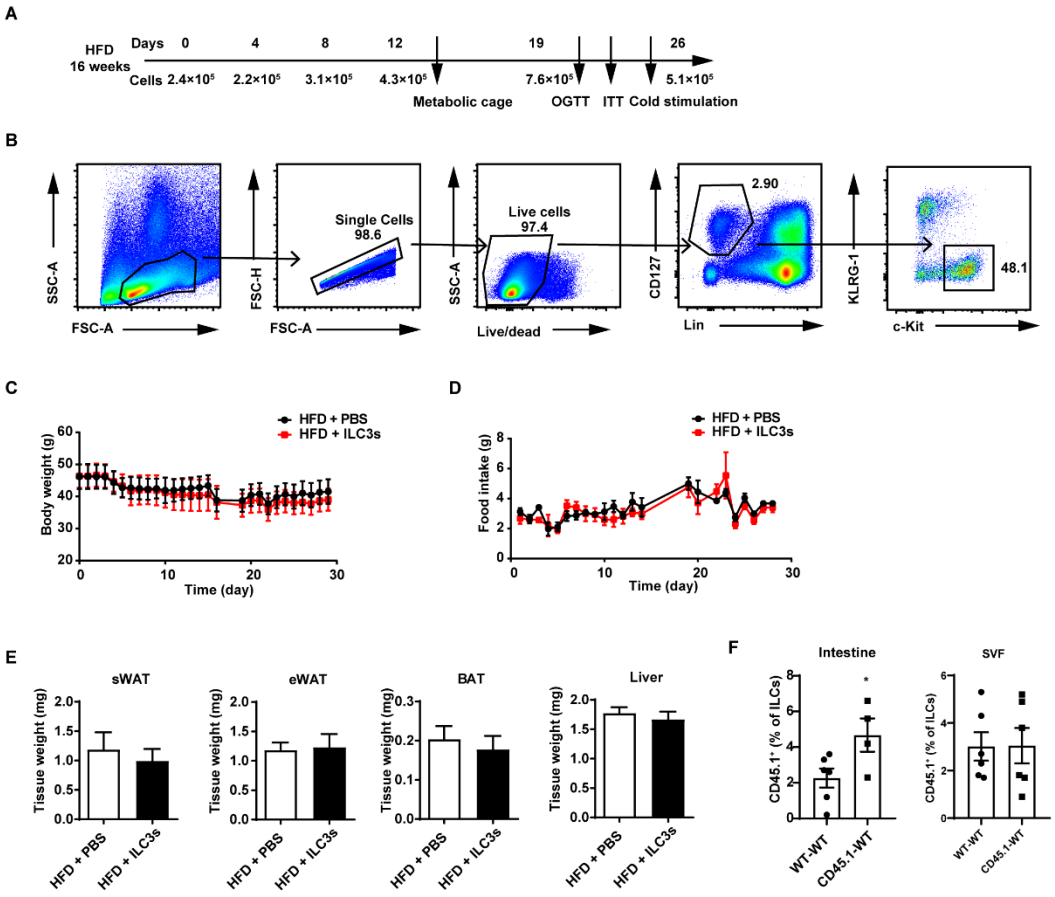

947

948 **Supplementary Figure 5 Adoptive transfer of ILC3s has no effect on the body**

949 **weight in mice fed HFD.**

950 A. Timeline for the recipient mice transferred with PBS or ILC3s. Mice were fed with

951 HFD for 16 weeks and then injected with ILC3s intravenously six times in a month.

952 B. Gating strategy for flow sorting of live CD127^{+} lineage^{-} c-kit^{+} KLRG1^{-}ILC3s in the

953 siLP.

954 C. Body weight of HFD mice transferred with ILC3s or control. n=6 per group.

955 D. Food intake of HFD mice transferred with ILC3s or control. n=6 per group.

956 E. Tissue weight of sWAT, eWAT, BAT, and liver from HFD mice transferred with

957 ILC3s or control. n=6 per group.

958 F. Transfer of ILC3s from CD45.1 mice to WT mice. The percentage of CD45.1+ cells

959 in ILCs in the small intestine and SVF. n=4-6.

960 All data represent the mean ± s.e.m. Statistical significance was determined by unpaired

961 two-tailed Student's *t* test.

962

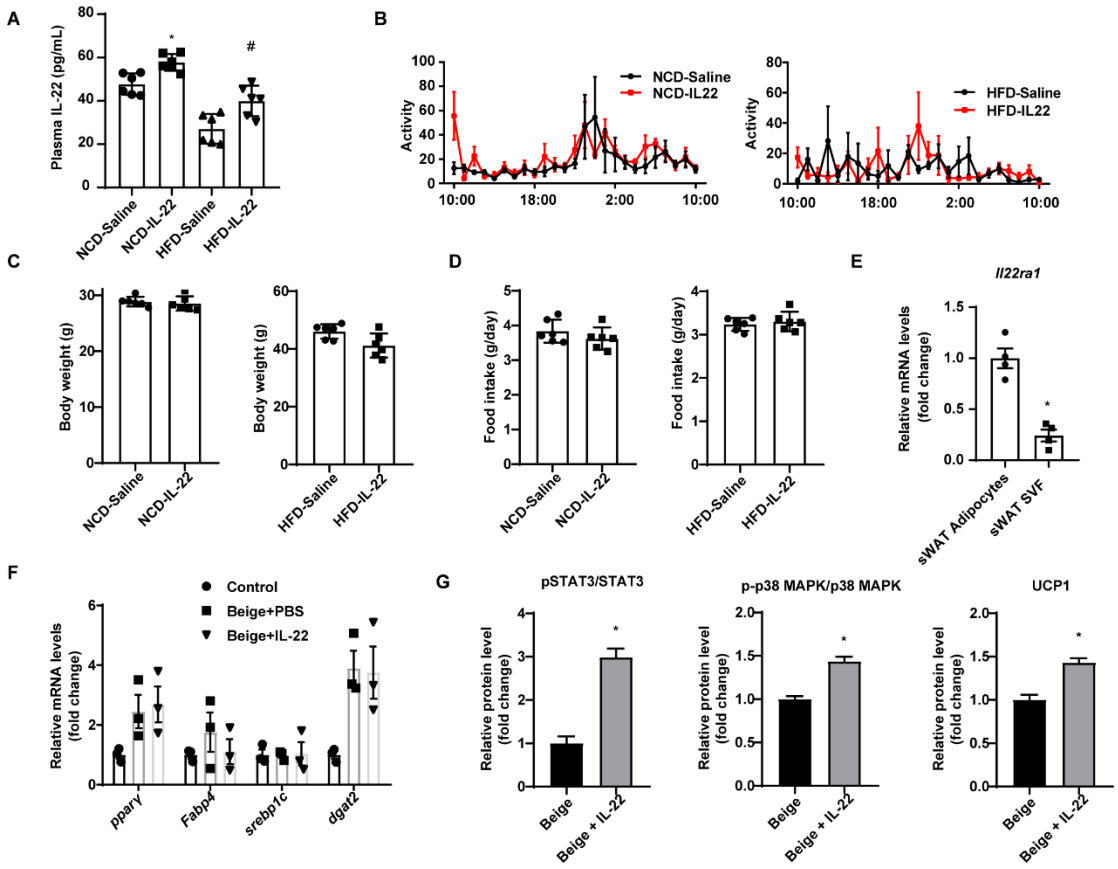

963

964 **Supplementary Figure 6 Exogenous IL-22 has no effect on the body weight of mice.**

965 A. Levels of IL-22 in plasma of NCD-Saline, NCD-IL-22, HFD-Saline, HFD-IL-22

966 mice. n=6 mice/group. # vs HFD-Saline.

967 B. Activity of mice fed NCD or HFD which were intraperitoneally injected with IL-22
968 or saline. n=5 for each group.
969 C. Body weight of NCD and HFD mice intraperitoneally injected with IL-22 or saline.
970 n=6 for each group.
971 D. Daily food intake of NCD and HFD mice intraperitoneally injected with IL-22 or
972 saline. n=6 for each group.
973 E. qPCR analysis of *Il22ra1* genes in adipocytes or SVF cells isolated from sWAT. n=4.
974 * denotes P<0.05 vs sWAT adipocytes.
975 F. qPCR analysis of adipogenic marker genes of SVF cells and adipocytes. n=3.
976 G. Relative protein signal intensity quantified using Image J software.
977 All data represent the mean ± s.e.m. Statistical significance was determined by one-
978 way ANOVA (A, F) with Bonferroni's multiple-comparisons test or unpaired two-tailed
979 Student's *t* test (B-E,G).

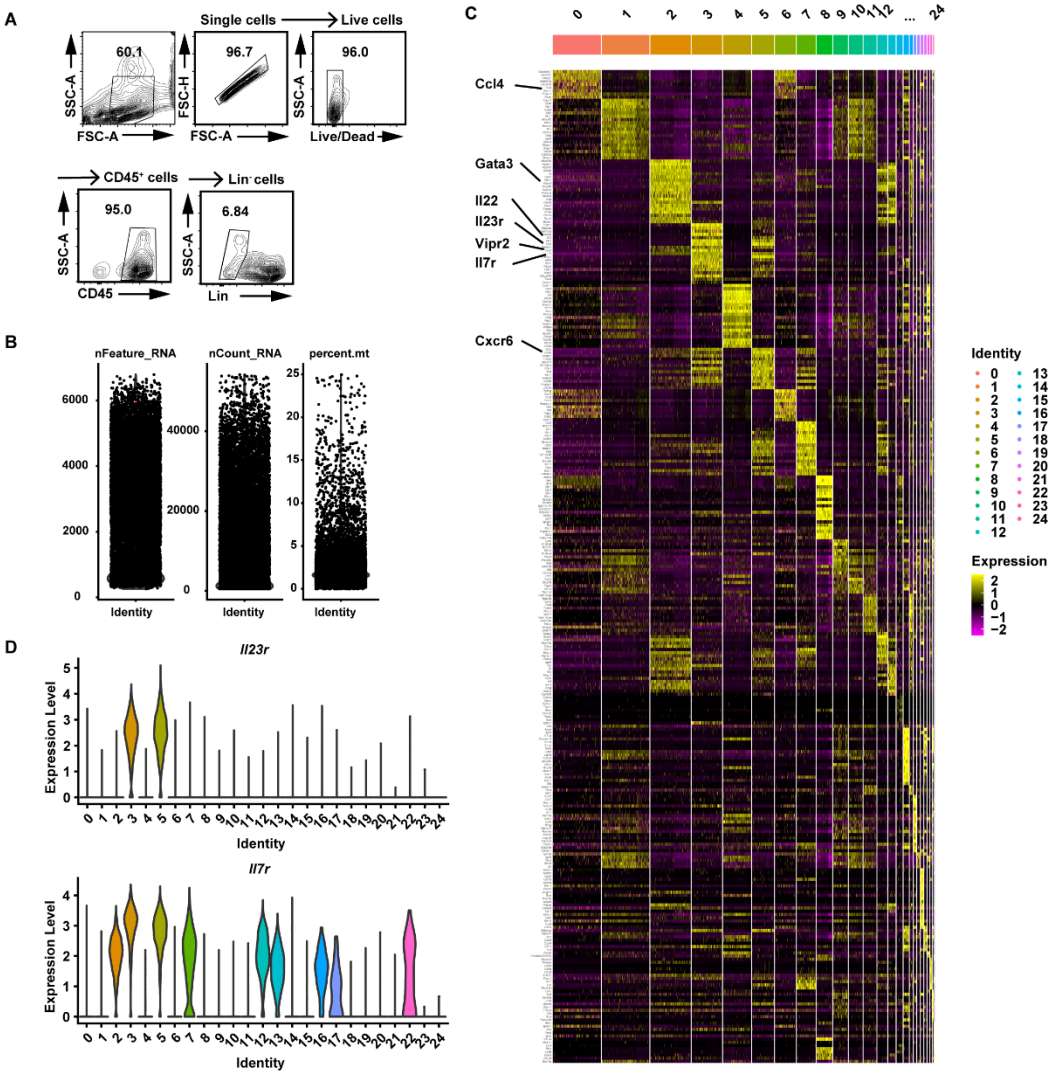

Supplementary Figure 7 Profiling of intestinal immune cells from mice fed NCD, HFD or HFD-IF

A. Gating strategy for flow cytometry sorting of Live CD45^{+} Lineage^{-} immune cells in the small intestine lamina propria.

B. scRNA-seq data quality control of sorted immune cells from mice fed NCD, HFD or HFD-IF.

C. Unbiased heatmap of the gene levels of the top 20 unique cluster marker genes for each cell cluster. Cluster identities are shown above the heatmap.

D. Violin plots showing RNA expression of cluster markers for the indicated cell

populations. UMAP feature plots are based on the UMAP shown in Figure 6A.

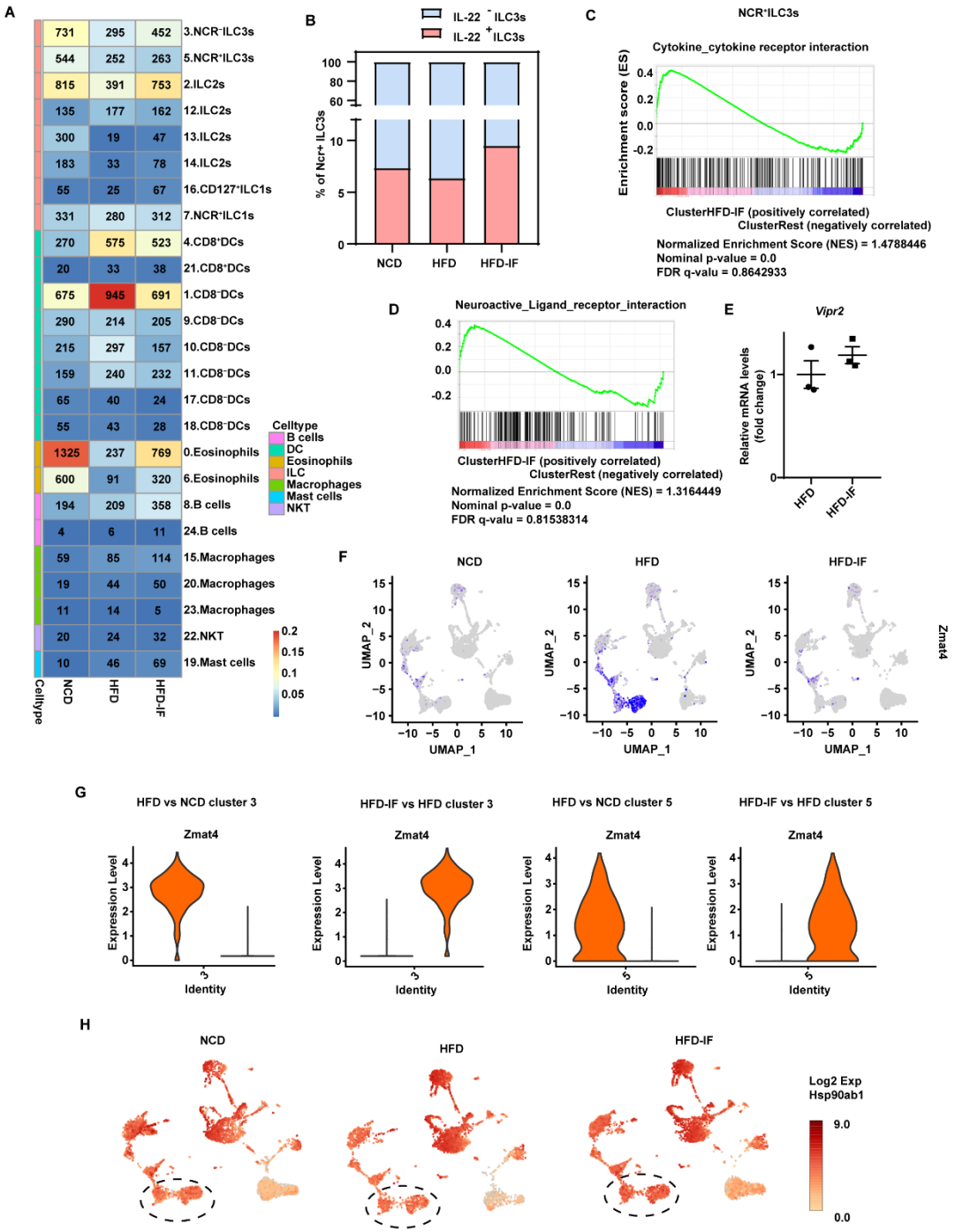

Supplementary Figure 8 Effects of Intermittent fasting on the gene expression of ILC3s.

A. Number and proportion of cells detected in each group in the study. Shown are Fraction (color bar, out of all cells from that group) and number of cells from each of

996 the 25 cell clusters (rows) in each individual group (columns).

997 B. Percentage of IL-22^{+} cells defined by the mRNA levels using Loupe Browser 5.0 of

998 NCR^{+} ILC3s in NCD, HFD and HFD-IF mice.

999 C. GSEA demonstrating enrichment of cytokine-cytokine receptor interaction pathway

1000 genes upregulated by intermittent fasting (HFD-IF mice) vs. control (HFD mice) in

1001 NCR^{+} ILC3s.

1002 D. GSEA demonstrating enrichment of neuroactive ligand-receptor interaction pathway

1003 genes upregulated by intermittent fasting (HFD-IF mice) vs. control (HFD mice) in

1004 NCR^{+} ILC3s.

1005 E. qPCR analysis of *Vipr2* in ILC3s sorted from siLP of HFD or HFD-IF mice.

1006 F. UMAP feature plots showing RNA expression of Zmat4 based on the UMAP shown

1007 in Figure 6B.

1008 G. Violin plots showing RNA expression of Zmat4 in NCR^{-}ILC3s (cluster 3) and

1009 NCR^{+}ILC3s (cluster 5).

1010 H. UMAP feature plots showing RNA expression of Hsp90ab1 based on the UMAP

1011 shown in Figure 6B.

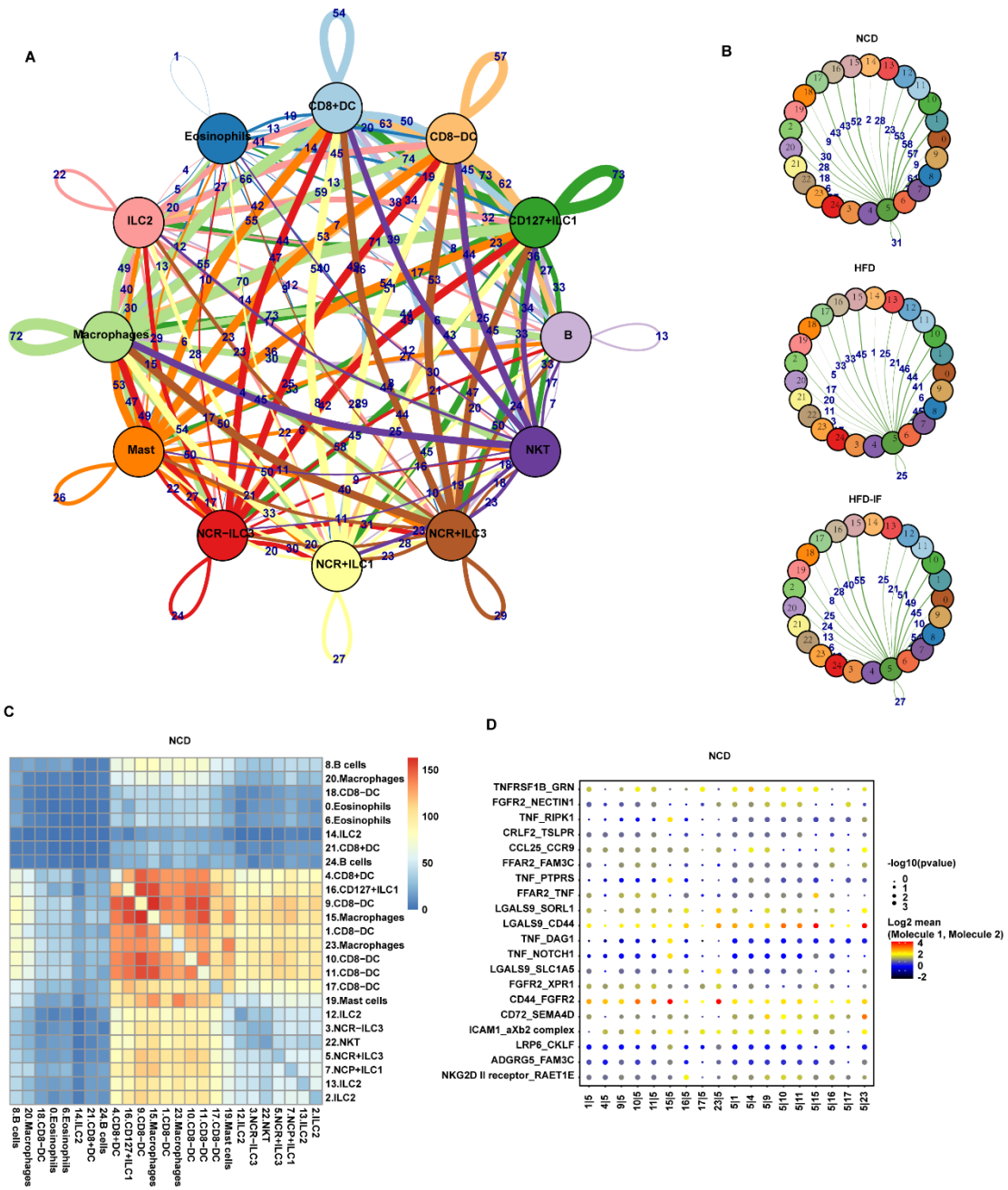

Supplementary Figure 9 Cell–cell interactions in the intestine.

A. Connectome web analysis of intestine immune cell interacting cell types based on the expression of the ligand in mice fed NCD. The vertex (colored cell node) represents the cell cluster. The thickness of the connecting lines is proportional to the number of interactions between the nodes.

B. Connectome web analysis of NCR^{+} ILC3s with the 25 cell clusters based on

expression of the ligand. The vertex (colored cell node) represents the cell cluster, while the thickness of the connecting lines is proportional to the number of interactions between two nodes.

C. Heatmap showing the number of significant interactions identified between cell types in sorted siLP immune cells of NCD mice as determined by CellphoneDB. The color represents the number of interactions between cell types: a higher number of interactions (red) and a lower number of interactions (blue).

D. Interaction pattern of the top 20 protein pairs and the top 20 cell types. The x-axis is the cell type interaction, and the y-axis is the protein interaction. The larger the point is, the smaller the p value. The color represents the average expression. Red to black indicates the level from high to low.

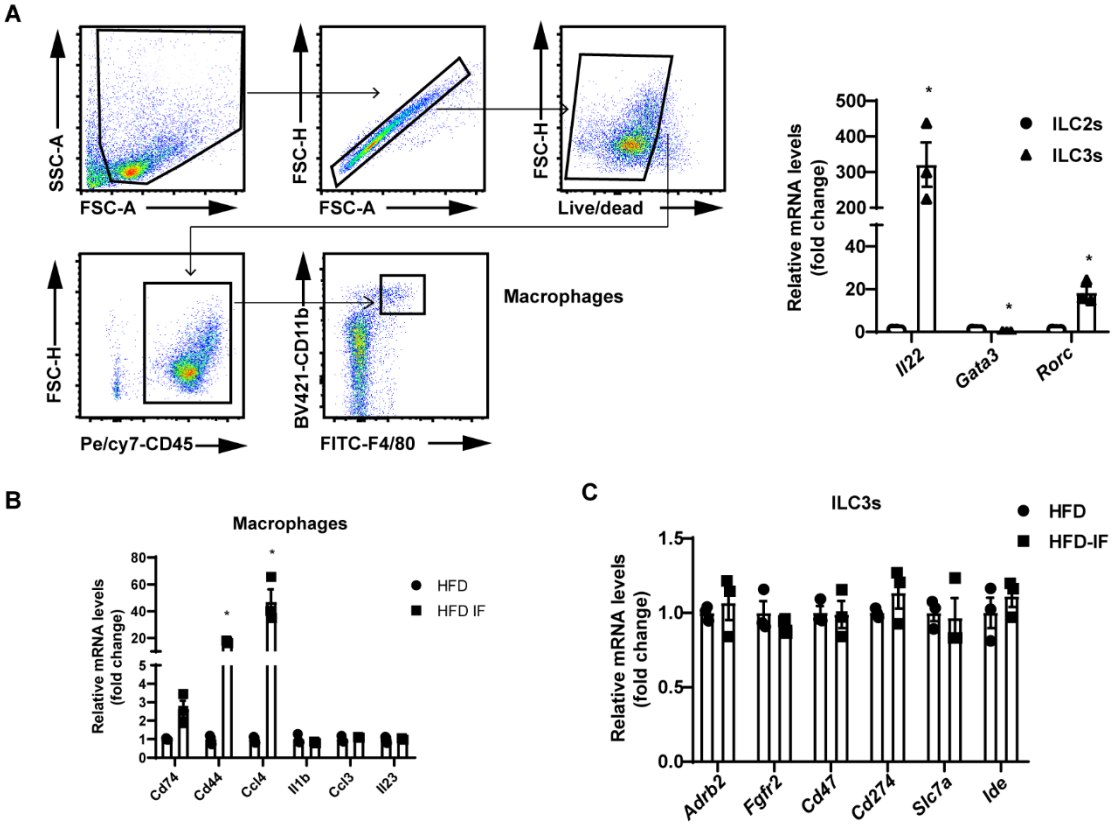

Supplementary Figure 10 Increased expression of CD44 and CCl4 in macrophages.

1032 Flow cytometry sorted macrophages and ILC3s from HFD and HFD-IF mice were used
1033 to detect the mRNA levels of proteins involved in the interaction of macrophages and
1034 ILC3s.
1035 A. Gating strategy for flow sorting of macrophages in the siLP. qPCR analysis of *Il22*,
1036 *Gata3*, and *Rorc* in ILC2s and ILC3s. n=3/group.
1037 B. mRNA levels of proteins involved in the interaction and *Il23* in macrophages.
1038 n=3/group.
1039 C. mRNA levels of proteins involved in the interaction in ILC3s. n=3/group.
1040 All data represent the mean ± s.e.m. Statistical significance was determined by unpaired
1041 two-tailed Student's *t* test.
1042
1043 **Table S1. Sequences of primers used in quantitative PCR.**

Gene	**Forward Primer**	**Reverse Primer**
Il22	ATGAGTTTTTCCCTTATGGGGAC	GCTGGAAGTTGGACACCTCAA
Il17	TCCCTCTGTGATCTGGGAA	CTCGACCCTGAAAGTGAAGG
Il1β	CCTTCCAGGATGAGGACATGA	TGAGTCACAGAGGATGG-GCTC
Il6	TAGTCCTTCCTACCCCAATTTCC	TTGGTCCTTAGCCACTCCTTC
Ifnγ	ATGAACGCTACACACTGCATC	CCATCCTTTTGCCAGTTCCTC
Tbp	ACCTTATGCTCAGGGCTTGG	GCCGTAAGGCATCATTGGAC
RpL32	GAGCAACAAGAAAACCAAGCA	TGCACACAAGCCATCTACTCA
Hprt2	TCAGTCAACGGGGGACATAAA	GGGGCTGTACTGCTTAACCAG
Hsl	CCAGCCTGAGGGCTTACTG	CTCCATTGACTGTGACATCTCG
Adrb3	GGCCCTCTCTAGTTCCCAG	TAGCCATCAAACCTGTTGAGC

Chrebpβ	AGATGGAGAACCGACGTATCA	ACTGAGCGTGCTGACAAGTC
Dio2	AATTATGCCTCGGAGAAGACCG	GGCAGTTGCCTAGTGAAAGGT
Atp1a2	CCACCACTGCGGAAAATGG	GCCCTTAGACAGATCCACTTGG
Atgl	AACACCAGCATCCAGTTCAA	GGTTCAGTAGGCCATTCCTC
Fabp4	ACACCGAGATTTCCTTCAAACTG	CCATCTAGGGTTATGATGCTCTTCA
Cidea	ATCACAACTGGCCTGGTTACG	TACTACCCGGTGTCCATTTCT
Ppargc1α	GATTGAAGTGGTGTAGCGAC	GTCGCTACACCACTTCAATC
Pparg	TCAGCTCTGTGGACCTCTCC	ACCCTTGCATCCTTCACAAG
Adrb3	GGCCCTCTCTAGTTCCCAG	TAGCCATCAAACCTGTTGAGC
Prdm16	CAGCACGGTGAAGCCATTC	GCGTGCATCCGCTTGTG
Il4	GGTCTCAACCCCCAGCTAGT	GCCGATGATCTCTCTCAAGTGAT
Ucp1	CACCTTCCCGCTGGACACT	CCCTAGGACACCTTTATACCTAATGG
Il23a	ATGCTGGATTGCAGAGCAGTA	ACGGGGCACATTATTTTAGTCT
Tnf	CGTCGTAGCAAACCACCAAG	GAGATAGCAAATCGGCTGACG
Adrb2	GGGAACGACAGCGACTTCTT	GCCAGGACGATAACCGACAT
Fgfr2	CCTCGATGTCGTTGAACGGTC	CAGCATCCATCTCCGTCACA
Cd47	TGGTGGGAAACTACACTTGCG	CGTGCGGTTTTTCAGCTCTAT
Cd274	GCTCCAAAGGACTTGTACGTG	TGATCTGAAGGGCAGCATTTC
Slc7a1	CTGCCTCAACACCTATGACCT	GAGAGCAGCAATCAAGAAGGAG
Ide	AATCCGGCCATCCAGAGAATA	GGGTCTGACAGTGAACCTATGT
Cd74	AGTGCGACGAGAACGGTAAC	CGTTGGGGAACACACACCA
Cd44	TCGATTTGAATGTAACCTGCCG	CAGTCCGGGAGATACTGTAGC

Ccl4	TTCCTGCTGTTTCTCTTACACCT	CTGTCTGCCTCTTTTGGTCAG
Il1b	GCAACTGTTCCTGAACTCAACT	ATCTTTTGGGGTCCGTCAACT
Ccl3	TTCTCTGTACCATGACACTCTGC	CGTGGAATCTTCCGGCTGTAG
Gata3	CTCGGCCATTCGTACATGGAA	GGATACCTCTGCACCGTAGC
Rorγt	GACCCACACCTCACAAATTGA	GACCCACACCTCACAAATTGA

1044

1045 **Table S2. Key resources**

Antibody and clone	**Source**	**cat#**
Cell Staining Buffer	BioLegend	420201
eBioscience^{TM} Fixation/Perm Diluent	Invitrogen	00-8333-56
eBioscience^{TM} Fixable Viability Dye eFluor^{TM} 606	Invitrogen	65-0866-14
PerCP/Cy5.5 anti-mouse CD45(30-F11)	BioLegend	103131
FITC anti-mouse CD3ε(RA3-6B2)	BioLegend	103205
FITC anti-mouse/human CD45R/B220(RA3-6B2)	BioLegend	103205
FITC anti-mouse Ly-6G/Ly-6C(Gr-1)(RB6-8C5)	BioLegend	108405
FITC anti-mouse CD19(6D5)	BioLegend	115506
FITC anti-mouse CD5(53-7.3)	BioLegend	100605
BV421 anti-mouse CD127(IL-7Rα) (A7R34)	BioLegend	135023
PE/Cyanine7 anti-mouse CD90.2(30-H12)	BioLegend	105325
PE/Cyanine7 anti-mouse CD45.1	BioLegend	110729
PE anti-mouse RORγt(Q31-378)	BD Pharmingen	562607
Alexa Fluor 647 anti-mouse IL-22(Poly5164)	BioLegend	516406
BV605 anti-mouse/human KLRG1(MAFA)(2F1/KLRG1)	BioLegend	138419
PE anti-mouse CD117(c-kit) (2B8)	BioLegend	105807
Rb polyclonal antibody to UCP1	abcam	ab10983
Phospho-Stat3 (Tyr705) Rabbit mAb	Cell signaling technology	#9145
Stat3 (124H6) Mouse mAb	Cell signaling technology	#9139
Phospho-p38 MAPK (Thr180/Tyr182) (D3F9) XP® Rabbit mAb	Cell signaling technology	#4511
p38 MAPK (D13E1) XP® Rabbit mAb	Cell	#8690

	signaling technology	

1046